

Universitat Politècnica de València

ESCUELA TÉCNICA SUPERIOR DE INGENIERÍA INDUSTRIAL

Master Universitario en Ingeniería Industrial



Structural Analysis and Optimization of a Space Module

Developed at Politecnico di Milano, Department of Aerospace Science and Technology, as part of an international exchange.



**POLITECNICO
MILANO 1863**

Supervisor at Universitat Politècnica de València:

Prof. Vicent Giner Bosch

Supervisor at Politecnico di Milano:

Prof. Sergio Ricci

Author:

Laura Feria del Rosario

Academic Year 2020-2021

Abstract

Designing light-weight aerospace structures without compromising structural integrity has historically been a strong driving force behind the development of optimum design methods. The main goal of this thesis work is to check the capability of the Finite Element solver OptiStruct from HyperWorks suite, from Altair Engineering in order to optimize design of a curved panel forming a space module.

This structure is a pressurized manned module designed by the company Thales Alenia Space. It is in a habitable module devoted to be part of a space station, consisting of a single compartment with two bulkhead-hatch systems which provide connection with other two modules, one of which being an airlock. The design of the cylindrical panels of the module is object of study.

In particular, stiffening of this plate is analysed so that mechanical requirements derived from design loads are fulfilled with the lightest design possible. For this purpose, OptiStruct optimization options (free-size, topology, topography and free-shape) are investigated in order to obtain the method providing the lightest feasible panel design.

Design loads include maximum expected accelerations and pressure during its whole life-time. This means that primary structure of the module is designed to withstand loads during handling, transportation, testing, launch, flight, on-orbit docking, berthing and on-orbit. Several constraints are involved: normal modes and yielding and buckling failure modes. Uncertainties in the space program (e.g., stability of the mass budget, well defined design) and the mathematical model used to represent the structure are considered in the optimization by applying factors of safety provided by European Space Agency standards.

Two approaches are followed to obtain the optimized panel design: optimization of the unstiffened and reinforced panel.

In the first case, thickness results are compared with equivalent optimization process performed in the same model in HyperSizer, another optimization tool. For this approach, the model used is the space module model itself composed by cylinder panels. Free-size method is employed. Differences in results show distinct capabilities of both tools used.

For the second approach, a stiffening panel optimization process is performed applying topology, topography and free-shape methods. Output reinforcement designs have distinct characteristics and shapes that are usable for an early design stage in order to define topology of stiffeners, depending on designer's priority.

Acknowledgements

I thank my thesis supervisors Prof. Sergio Ricci from the Aerospace Department of Engineering at Politecnico di Milano and Prof. Vicent Giner Bosch from Universitat Politècnica de València. Their active support and help during this project were indeed crucial. Thanks to them this thesis has become a priceless educational experience.

I am also grateful for my family and friends for supporting me and encouraging me along the way, but especially in the hardest days.

In addition, I want to address thanks to Altair Engineering who has generously provided a full software license and access for courses and tutorials in how to use the software (HyperMesh, OptiStruct and HyperView). Altair Engineering has also assisted with technical support in the best possible way.

Content

Abstract	i
Acknowledgements	ii
List of figures	v
List of tables	vii
Acronyms	viii
1 Introduction	1
1.1 Context and motivation	1
1.2 Objectives.....	1
1.3 Scope and limitations	1
1.4 Thesis outline	2
2 Optimization process.....	3
2.1 Structural optimization.....	3
2.2 Optimization problem	3
2.3 Types of optimization problems.....	4
3 OptiStruct features.....	5
3.1 OptiStruct capabilities	5
3.2 Optimization process.....	5
3.3 OptiStruct optimization types.....	6
3.4 Manufacturing constraints.....	10
3.5 Convergence.....	11
3.6 OSSmooth	11
4 Structure description	12
4.1 Components.....	12
4.2 Coordinate system.....	16
4.3 Material	17
4.4 Finite element model.....	17
4.5 Constrains.....	18
5 Mechanical requirements and failure modes.....	19
5.1 Limit Loads	19
5.2 Panel stability	19
5.3 Primary modes	19
5.4 Subcases	20
5.5 Design Limit Loads.....	20
5.6 Failure modes	21
6 Preliminary analyses	24

6.1	Analysis set up	24
6.2	Results	25
7	Optimization of an unstiffened curved panel	32
7.1	Optimization set up	32
7.2	Results	33
7.3	Normal modes analysis	36
7.4	Comparison of optimization results with HyperSizer	37
8	Optimization of a reinforced curved panel.....	39
8.1	Optimization model.....	39
8.2	Finite element model for the panel.....	40
8.3	Free size optimization	41
8.4	Topology optimization	41
8.5	Topography optimization	45
8.6	Free-shape optimization	49
9	Conclusions	55
Appendix A.	Finite element model of module.....	57
References	61

List of figures

Figure 2.1. Types of structural optimization problems [3].....	4
Figure 3.1. HyperWorks workflow	5
Figure 3.2. Transition zone grids [4].....	7
Figure 3.3. Bead parameters [4].....	8
Figure 3.4. Buffer zone [4].....	9
Figure 3.5. Check boarding: (a) Design problem, (b) Checkerboards [7].....	10
Figure 4.1. Lateral view of module's primary structure [1].....	13
Figure 4.2. Top view of module's primary structure [1].....	13
Figure 4.3. Bottom view of module's primary structure [1]	14
Figure 4.4. Front view of module's primary structure [1]	15
Figure 4.5. Example of secondary masses allocation [1]	15
Figure 4.6. Schematic representation of secondary masses (in blue) between longerons (in red) [1]	16
Figure 4.7. Module's coordinate system [1]	17
Figure 4.8. Lateral view of the FE model [1]	18
Figure 4.9. Constrained nodes [1]	18
Figure 6.1. Module's area of study [1]	24
Figure 6.2. Maximum von Mises stresses [Pa] for quasi-static loads (subcase 8)	26
Figure 6.3. Maximum von Mises stresses [Pa] for pressure loads (subcase 9)	27
Figure 6.4. Buckling shape for subcase 2 with displacement contour (m).....	28
Figure 6.5. Mode 1 (first lateral mode) deformed representation (x10) and mass normalized displacement contour (m).....	29
Figure 6.6. Mode 2 (second lateral mode) deformed representation (x10) and mass normalized displacement contour (m).....	30
Figure 6.7. Mode 4 (first longitudinal mode) deformed representation (x10) and mass normalized displacement contour (m).....	31
Figure 7.1. Optimization model [1].....	32
Figure 7.2. Buckling shape for subcase 2 after optimization with displacement contour (m)	34
Figure 7.3. Maximum von Mises stress [Pa] after optimization for pressure loads (subcase 9) .	35
Figure 8.1. Panel dimensions	39
Figure 8.2. Panel finite element model	40
Figure 8.3. Panel connections	41
Figure 8.4. Rib pattern definition for topology optimization [4]	42
Figure 8.5. Topology ptimized panel. Element density values from 0 to1	43
Figure 8.6. Buckling shapes for subcase 7 after topology optimization with displacement contour (m).....	44
Figure 8.7. Envelope of maximum von Mises stress [Pa] for topology optimization (subcase 9)	44
Figure 8.8. Topography optimization shape changes [m]	47
Figure 8.9. Buckling shapes for subcase 7, case (B), along topography optimization with displacement contour (m).....	48
Figure 8.10. Topography optimization stress results [Pa].....	48
Figure 8.11. Linear manufacturing constraint example [4].....	49
Figure 8.12. Free-shape optimization shape changes [m]	52
Figure 8.13. Buckling shapes for 4-layer model after free-shape optimization (subcase 7)	53
Figure 8.14. Free-shape optimization stress results for 4-layer model [Pa] (subcase 9).....	53
Figure A.1. Lateral view of the FE model [1].....	58

Figure A.2. Top view of the FE model [1]	58
Figure A.3. Detailed view of longerons attachments and secondary masses connections [1].....	59
Figure A.4. Detailed view of CBUSH elements (in white) [1].....	60

List of tables

Table 4.1. Aluminium 2219-T851 properties.....	17
Table 5.1. Quasi-Static Limit Loads	19
Table 5.2. Subcases	20
Table 5.3. Factors of safety	21
Table 6.1. Preliminary stress and buckling results	25
Table 6.2. Modal preliminary analysis results	28
Table 7.1. Buckling analysis results for optimized and baseline models	33
Table 7.2. Yield strength analysis results for optimized and baseline models	34
Table 7.3. Modal analysis results for optimized module	36
Table 7.4. Modal analysis difference results. Values refer to difference between optimized model minus baseline results	37
Table 7.5. Buckling analysis results obtained in [1] (Table 5.6).....	38
Table 7.6. Strength analysis results obtained in [1]	38
Table 8.1. Constraints for panel FE model.....	41
Table 8.2. Stiffened (topology) vs unstiffened (free-size) panel optimization results	43
Table 8.3. Cases of study for topography optimization	46
Table 8.4. Results for topography optimizations	46
Table 8.5. Results for free-shape optimizations	50
Table A.1. FE model summary.....	57

Acronyms

CAD	Computer Aided Design
DLL	Design Limit Loads
DOF	Degree Of Freedom
FE	Finite Element
FEA	Finite Element Analysis
FEM	Finite Element Method
FOS	Factor Of Safety
FOSB	Buckling Factor of Safety
FOSY	Yield design Factor Of Safety
KDF	Knock Down Factor
K_M	Model factor
K_P	Project factor
MOS	Margin Of Safety

1 Introduction

1.1 Context and motivation

In aerospace industry, there is a need of minimizing spacecraft structural weight in order to increase launchers payload capabilities, as it is one of the major contributors to spacecraft dry mass. Design of light-weight structures which does not compromise mechanical integrity, has historically been a strong driving force behind the development of optimum design methods. Especially, design of reinforced panels has been considerably researched. This interest is due to the fact that launch vehicle stages, propellant tanks, pressurized modules, and many other aerospace structures consist mostly of those.

However, majority of research is done in some typical stiffening designs, e.g., panels with an orthogrid waffle internal reinforcement. In general, optimization tools are limited for the need of input parameters that already constrain final optimized designs. An automated variation of optimization input parameters is necessary to get this approach.

OptiStruct is a finite element solver which can conduct optimizations as well. It belongs to the HyperWorks suite from Altair Engineering, and it is a powerful finite element optimization tool because of its wide variety of optimization methods.

Therefore, OptiStruct is a good candidate for allowing structure designer not to restrict himself for predefined stiffening shapes, but is it able to produce a reinforcement pattern without any predefined limitation? In order to answer this ultimate question, optimization methods available in OptiStruct must be studied.

1.2 Objectives

The main purpose of this thesis work is to determine OptiStruct capabilities for the optimization of a curved panel used in a space module. However, it can be subdivided into two objectives. The first goal is to compare optimization process and results for an unstiffened curved panel performed by OptiStruct and HyperSizer. Optimization for the former solver is done as part of the present thesis. Results for the latter software are obtained from another master thesis written by Virtudes de Gregorio Roig for Politecnico di Milano [1].

The second objective is to determine whether OptiStruct is capable of generating an optimized stiffened panel with minimum design parameter limitations that fulfils established structural requirements. For this purpose, the different optimization methods included in OptiStruct are studied.

1.3 Scope and limitations

The object of study is a curved panel of a space module. Finite element model is provided by Thales Alenia Space. However, different models are used for both approaches made along this work.

In order to compare OptiStruct optimization with results obtained in [1], the complete space module model is used, so that finite element model is the same in both studies. Optimization is performed in the unstiffened panel that forms the primary structure of the space module. This study is part of a preliminary design phase. The resulting design can be used to perform a preliminary mass estimation and assessment of the module structure primary frequencies as part of the mission design.

1. Introduction

For the second approach, optimization with the different methods provided by OptiStruct is applied to a single cylinder panel. Geometry is extracted from previous space module primary structure. In this way, it is possible to simplify Finite Element Analysis (FEA) to investigate OptiStruct capabilities. The obtained results will give an initial idea of where to locate and how to define reinforcements in a curved panel. It is not part of a preliminary design mission phase.

From the curved panel, only stiffening strategies are studied, so areas close to the edges of the curved panel will not be case of research as they are extremely conditioned by joining techniques between adjacent components.

1.4 Thesis outline

The present thesis document is organized in 9 sections. The current section includes the context and motivation of this thesis work as well as the scope and the objectives. Section 2 gives an overview of how optimization is applied to structural designs. In section 3, a summary of OptiStruct features and capabilities is developed. Section 4 is devoted to the description of the structure which is object of study, including its geometry, material and principal information related to finite element model. In section 5, design mechanical requirements, that structure object of study must fulfils, are described and associated to specific failure modes to be prevented. Section 6 presents preliminary structural analyses results. Section 7 is devoted to the optimization formulation and results of the complete model. A comparison with preliminary results and those obtained in [1] is done. In section 8, different OptiStruct optimization methods are evaluated for optimizing a curved panel. Lastly, section 9 is devoted to the conclusion's discussion.

The present thesis document has one appendix. In Appendix A structure finite element model is thoroughly described.

2 Optimization process

2.1 Structural optimization

The purpose of structural optimization is to obtain the optimal material distribution according to some given demands of the structure. Typical objective functions are minimization of mass, displacement or compliance (strain energy). Constraints are usually related to mass, volume, size or failure.

Structural optimization is traditionally done manually using a 3-steps iterative-intuitive process [2]:

1. A structural design is suggested.
2. The mechanical requirements to be fulfilled are evaluated. This step is nowadays developed by means of computer-based methods like the Finite Element Method (FEM).
3. If requirements are met, the optimization process is finished. Otherwise, modifications are made, a new improved design is proposed and steps 2 and 3 are repeated.

Results and number of iterations depend to a large extent on designer's knowledge, experience and intuitive understanding of the problem. This is due to the fact that changes in design are made in an intuitive way, often using trial and error. For this reason, optimization process can be very time consuming and, finally, may result in a non-optimal design because some characteristics can still be improved.

So as to improve timing and results, a mathematical design optimization method is implemented so that steps 2 and 3 are automatically developed. OptiStruct is an optimization tool that can solve this type of problem.

2.2 Optimization problem

For every optimization process there are 5 elements that must be defined.

- *Design space*, includes parts which are designable during optimization process. The excluded parts are known as the non-design space.
- *Design variables*, are the system parameters that are varied to optimize performance.
- *Responses*, are the measurements of system performance, e.g., mass, volume, mass and volume fraction, temperature, stress, displacement, buckling factor or frequency. They can then be used either as an objective function or as a constraint.
- *Objective function*, represents the response function of the system to be optimized.
- *Constraint functions*, are the bounds on response functions of the system that must be satisfied for the design to be feasible.

The typical formulation for an optimization problem is the following one

$$\text{minimize} \quad f(x) = f(x_1, x_2, \dots, x_n) \quad i = 1, 2, \dots, n \quad (2.1)$$

$$\text{subject to} \quad g_j(x) \leq 0 \quad j = 1, 2, \dots, m \quad (2.2)$$

$$x_i^L \leq x_n \leq x_i^U \quad (2.3)$$

where $f(x)$ is the objective function, and $g_j(x)$ are the constraint functions. A constraint can be considered active if it is satisfied exactly ($g_j(x) = 0$); inactive if it is simply satisfied; and violated. Finally, x_n represents the design variables with their corresponding lower and upper limits (x_i^L, x_i^U).

2.3 Types of optimization problems

According to Christensen and Klarbring [2], there are three different types of structural optimization problems: sizing, shape and topology.

- *Sizing optimization* is the simplest form of structural optimization. It is performed when it is not necessary to remove materials, generate beads or change the shape of the structure, which is known. The objective is to optimize the structure by adjusting sizes of components, which are the design variables, e.g., cross-sectional areas of truss members, or the thickness distribution of a sheet. See Figure 2.1.(a) for an example of size optimization where shape is fixed and design variables correspond to diameter of rods.
- *Shape optimization* is developed by modifying the outer boundary of the structure. However, connectivity of the structure is not changed: new boundaries are not formed, e.g., new holes or split bodies will not appear. Shape variables are the design variables, and those could be, for instance, thickness distribution along structural members, diameter of holes or radii of fillets. A shape optimization problem is seen in Figure 2.1.(b).

A fundamental difference between shape vs. topology and size optimization is that instead of having one or more design variables for each element, in this case, design variables affect many elements.

- *Topology optimization* is the most general form of structural optimization. In this case, the resulting shape or topology is not known, the number of holes, bodies, etc., are not decided yet. The purpose is to find the optimum distribution of material and voids, a so called 0-1 problem, where material either exists or not. To solve this problem, structure is discretized by using FEM and dividing the design domain into discrete elements (mesh). An example is shown in Figure 2.1.c.

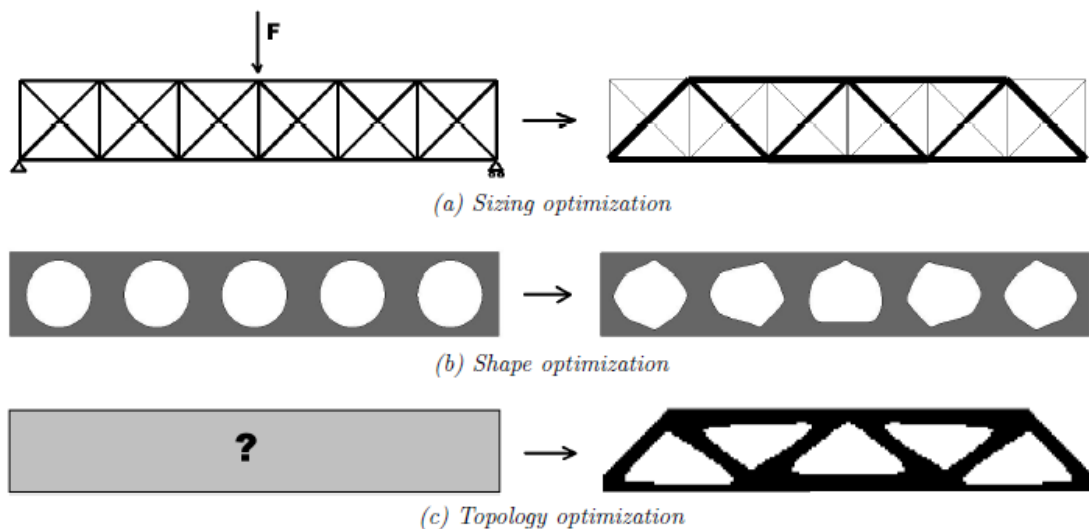


Figure 2.1. Types of structural optimization problems [3]

3 OptiStruct features

3.1 OptiStruct capabilities

OptiStruct is a solver which is capable of performing a range of finite element analyses; like static, modal, buckling and thermal analyses. Several types of loads such as point forces, pressure, gravitational loads, and thermal loads can be applied. In addition, many different types of elements are supported including: three-dimensional solid elements, two-dimensional shell elements and other elements such as beams, bars, springs and point masses.

Both, finite element analysis and optimizations, can be solved with OptiStruct. Moreover, there are different types of optimizations available based on the subdivision established for structural optimization in section 2.3.

- *Free-size optimization*, determines the optimal thickness distribution of shell elements.
- *Size optimization*, calculates the optimal design variables which affect the property of interest.
- *Free-shape optimization*, determines the optimal shape of a structure.
- *Shape optimization*, determines the optimal shape of a structure based on pre-defined boundaries created by the user.
- *Topography optimization*, finds the best reinforcement pattern of a shell structure.
- *Topology optimization*

More information about each optimization can be found in section 3.3 or in OptiStruct User's Guide [4].

3.2 Optimization process

OptiStruct does not have any graphical interface. For this reason, HyperMesh and HyperView were also used for this work. All of them are part of the software suite HyperWorks from Altair Engineering. HyperMesh is the pre-processor, which is used to create the mesh from a CAD model, set boundary conditions and set up the problem to be solved. Afterwards, HyperMesh exports a file which defines the problem so that OptiStruct can solve it. Finally, results can be reviewed in the HyperView post-processor. Figure 3.1 represents the workflow of HyperWorks.

All tools used for this work from HyperWorks suite correspond to 2021.1 version.

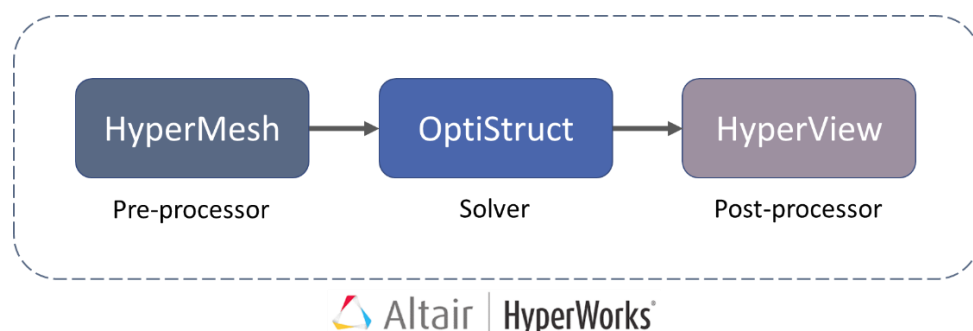


Figure 3.1. HyperWorks workflow

3. OptiStruct features

In general, the procedure for setting up an optimization problem to be solved in OptiStruct is roughly the same independently of the optimization type. It is mainly developed in HyperMesh. Steps to be followed are listed below.

1. Obtaining the Finite Element (FE) model. HyperMesh is capable of importing and creating linked geometry and FE model. For checking HyperMesh capabilities, please refer to [5].
2. Definition of design variables and their constraints.
3. Definition of responses that will be used as objective or constraints.
4. Formulation of optimization objective.
5. Set of constraints on responses. This step is not always necessary, it depends on each optimization problem.

For steps from 2 to 5, there are different possibilities and limitations for each optimization type. In the next section, some of them are mentioned, however in order to widen information, OptiStruct User's Guide [4] can be consulted.

3.3 OptiStruct optimization types

Free-size optimization

Free-size produces an optimized thickness distribution per element for a 2D structure. Several manufacturing constraints can be set in order to, for example, have uniform thickness for a group of elements.

Free-size stress constraints have some limitations that must be consulted in [4] previously, but for the scope of this work it is possible to add stress constraints by using the stress-NORM aggregation. The NORM method calculates the maximum value of a particular response of all the grids/elements grouped approximately.

The buckling factor can be constrained only if shells have a base thickness not equal to zero.

Moreover, OptiStruct has the capability of performing free-size optimization simultaneously with the other types of optimizations.

Free-size optimization is the process used in this work to obtain the optimized thickness for the curved panels of the pressurized module.

Size (parameter) optimization

Some structural elements have properties depending on several parameters; like beams whose area, moments of inertia, and torsional constants (properties) depend on the cross-section geometry (parameters). Those parameters are the design variables. The objective of size optimization is to adjust the design variables so that the property of interest is optimized.

These design variables can be set to take a continuous value, a discrete value or choose between a set of predefined values.

Furthermore, OptiStruct has the capability of performing size optimization simultaneously with the other types of optimizations.

Because of the scope of this work, sizing optimization will not be used. The only improvement with respect to free-sizing is that discrete thickness variables can be imposed in order to find the

3. OptiStruct features

commercial panel model that better fits the requirements. However, as this work is part of a preliminary design, this approach is not necessary.

Free-shape optimization

Free-shape optimization is an automated way to modify the structure shape based on set of nodes that can move totally free on the boundary to find the optimal shape. The allowable movement of the outer boundary is automatically determined, so it is not needed that user defines those boundaries for the shape variables. It is sufficient to choose a set of nodes on the boundary.

During a classic free-shape optimization, the outer boundary of a structure is modified to meet objectives and constraints. Depending on the element property, the design grids can move in one of two ways:

1. For shell structures, grids move normal to the surface edge in the tangential plane.
2. For solid structures, grids move normal to the surface.

It is remarkable that the normal directions are modified with the change in shape of the structure; i.e., design grids move along the updated normals for each iteration.

It is possible to classify nodes taking part in free-shape optimization in three groups: the non-design nodes, the design nodes and those in the transition zone. The nodes in the transition zone will be adjusted during free-shape optimization to build a smooth transition between "non-design nodes" and "design nodes", in order to prevent discontinuous or sharp sections to occur.

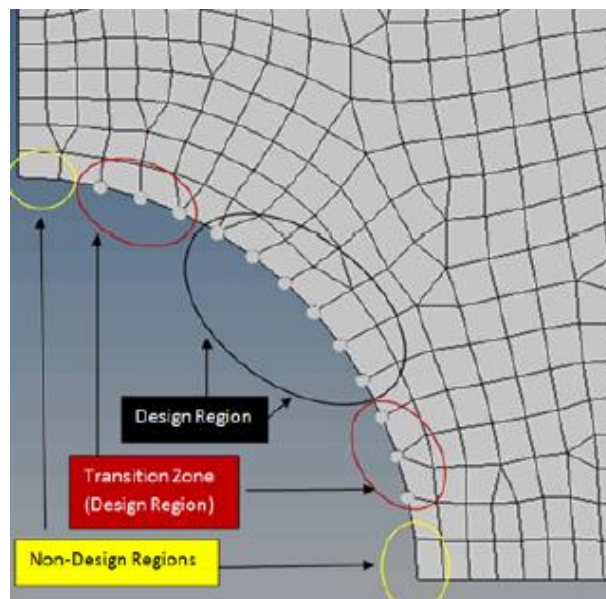


Figure 3.2. Transition zone grids [4]

There are five parameters that can be indicated to define the way in which the free-shape design region deforms.

- Direction type. It provides a constraint on the direction of design region movement; inside or outside of the initial boundary.
- Move factor. It affects the maximum movement of grids in one iteration.
- Number of layers for mesh smoothing. Internal grids adjacent to those forming the design region are moved to avoid mesh distortion. The number of layers of grids to be included

3. OptiStruct features

in the mesh smoothing buffer can be defined. A larger value will give a larger smoothing buffer; nevertheless, it will result in a slower optimization.

- Maximum shrinkage and growth, which limit the total amount of deformation of the free-shape design region.

Free-shape optimization will be used for checking OptiStruct capabilities in order to determine optimum stiffeners shape and position for the curved panels of the module.

Shape

Shape optimization is able to modify the structure shape based on user-predefined shape variables to find the optimal shape, on the contrary to free-shape process. Using finite element models, the shape is defined by the grid point locations. Then, shape optimization modifies these locations to update the shape.

To define design variables, firstly a shape is created by using a module in HyperMesh called Hypermorph. Then, a design variable is easily defined from the shape, together with bounds on maximum or minimum magnitude of the shape change.

Shape optimization will not be used in this work because user-predefined shapes are needed. Therefore, shapes generated are already limited that could result in a non-optimized solution and the objective of this work is to obtain different reinforcement patterns without any restriction in order to check whether traditional stiffeners patterns are the optimized ones.

Topography optimization

Topography is an advanced form of shape optimization in which a pattern of reinforcements within the design region is generated. To determine geometry of the shape variables it is necessary to define the following parameters: bead minimum width, draw angle in degrees and draw maximum height. Figure 3.3 shows a cross-section of a single shape variable normal to the plane of the design elements.

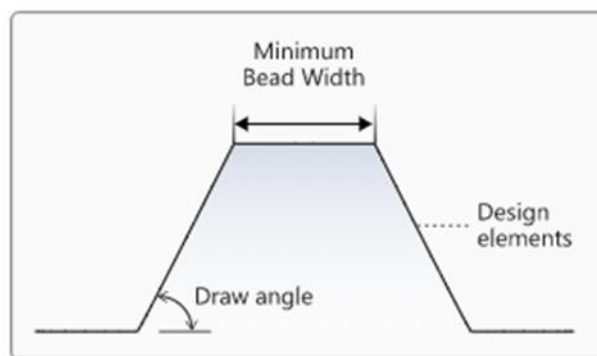


Figure 3.3. Bead parameters [4]

Shape variables can be generated following the element normal method, where beads are intended to be drawn normal to the surface; or the draw vector or the user-defined methods, where a specific direction is set for the extrusion of beads. Manufacturing constraints like pattern grouping, symmetry pattern, or linear draw direction can be used in order to produce a specific reinforcement pattern.

The buffer zone is a parameter that controls how the interfaces between design and non-design elements are treated. If active, OptiStruct will place the shape variables far enough away from the

3. OptiStruct features

non-design elements so that the proper bead widths and draw angles are maintained. If inactive, the boundary between the beads and non-design elements will have an abrupt transition. [4]

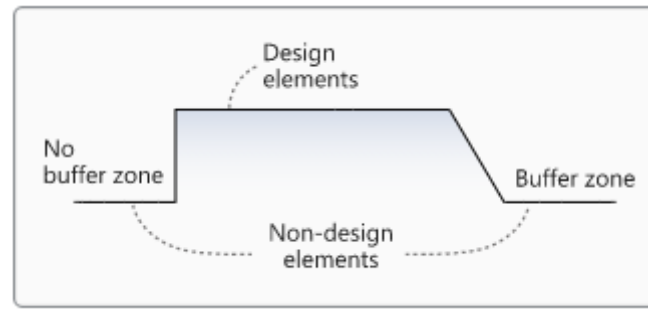


Figure 3.4. Buffer zone [4]

However, topography optimization has some restrictions, e.g., it is not recommended to have mass and volume responses as objectives or constraints since they are not very sensitive to shape changes. On the contrary, even though topography optimization is primarily a tool for creating bead type reinforcements in shell elements, it can accommodate solid models, as well.

Although topography optimization does not add material for creating the stiffeners, but only modifies the shape of the shell structure to improve its performance, it can help designer to determine the best position and orientation of stiffeners. Then, a new structure design can be developed following topography pattern results. Therefore, this type of optimization will be used in this work to get a first approach of possible stiffeners for the curved panels of the axial cylinder module.

Topology optimization

The purpose of topology optimization is to find the optimum distribution of material and voids. In this regard, for solid elements, results will be represented by its material density, which should take a value of either 0 or 1, defining the element as being either void or solid, respectively. Meanwhile for two-dimensional elements, thickness will be optimized i.e., zero or a fixed maximum element thickness. No other elements can be used as design variables.

It is desirable to achieve a discrete design, meaning a design where the vast majority of elements are either 0 or 1. Unfortunately, optimization of a large number of discrete variables is computationally prohibitive. Therefore, representation of the material distribution problem in terms of continuous variables must be used. The material density of each element is used as the design variable and varies continuously between 0 and 1. The stiffness of the material is assumed to be linearly dependent on the density.

Intermediate values of density are the transition zone and represent fictitious material. When large amounts of medium dense elements exist, interpretability is more difficult and the performance of the structure, reported at the end of the optimization, becomes inaccurate. Therefore, techniques need to be introduced to penalize intermediate densities and to force the final design to be represented by densities of 0 or 1 for each element. OptiStruct uses different penalization techniques in different settings of topology optimizations. Nevertheless, despite their low penalized stiffness, medium-dense elements can still have a significant influence on the structural behaviour. In consequence, a reanalysis after interpretation of the structure is recommended to verify its performance.

3. OptiStruct features

The transition zone is acceptable in most cases. But it should be avoided to have large areas containing mainly medium dense elements. For this reason, the amount of medium dense elements is calculated. A ratio between the volume from elements with densities of at least 0.9 and that of the entire design space is used. For a perfectly discrete model this value would be 1.0 but for structures where a transition zone exists, this parameter should be 0.5 or higher. When values are smaller than that at the end of the optimization, the topology should, at least, be interpreted with caution

It is important to remark that different properties must be used for design and non-design elements, where properties are defined using HyperMesh and describes an element by type, material, etc.

As for the free-size, for topology optimization, stress constraints have some limitations that can be consulted in [4], but for the scope of this work it is possible to add stress constraints by using the stress-NORM aggregation.

Likewise, the buckling factor can be constrained for shell topology optimization problems with a base thickness not equal to zero. Constraints on the buckling factor are not allowed in any other cases.

A common problem in topology optimization is checkerboarding. Checkerboarding refers to the checkerboard pattern that is formed when there are alternating elements with density of 1 and elements with density of 0. Is it due to exaggeration of element stiffness when they are connected to each other by just the corners [6]. This together with the common practice to use one design variable per element and using penalization of intermediate densities will lead to checkerboard patterns. So as to avoid this effect, OptiStruct recommends to set a minimum size member constraint as it is described in section 3.4.

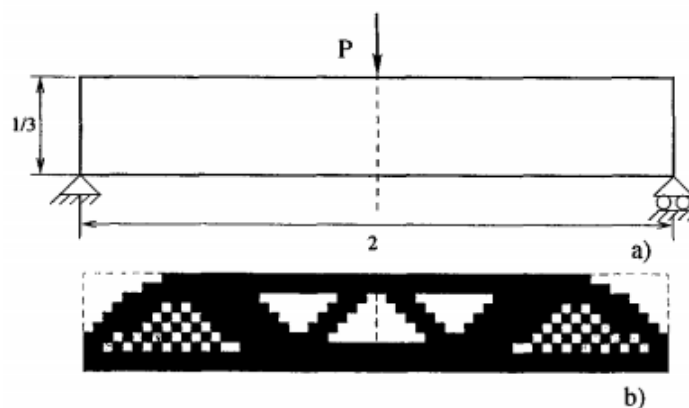


Figure 3.5. Check boarding: (a) Design problem, (b) Checkerboards [7]

3.4 Manufacturing constraints

The manufacturing constraints are additional inputs for the optimization problem which make interpretation of results easier. In this way, it is possible to constrain optimized design to be manufacturable with standard tools and processes. The main manufacturing constraints are listed below.

- *Member size control* can specify minimum or maximum dimension for members to be formed during optimization. When the smallest dimension is defined it controls checker board effect. It can be used in topology and free-size optimizations.

3. OptiStruct features

- *Side constraints*, in a similar way, allow the deformation space to be defined as a coordinate range during free-shape optimization. These ranges may be with reference to rectangular, cylindrical or spherical systems.
- *Pattern grouping and pattern repetition* can be applied to enforce a repeating pattern or symmetrical design even if the loads applied on the structure are unsymmetrical or non-repeating. Symmetry can be applied in 1, 2 or 3 planes or even cyclic symmetry (rotational). They can be used in all optimization types.
- *Draw direction constraints* can be applied to obtain design suitable for casting or machining operations. Constrained determined topology will allow the die to slide in a given direction by preventing cavities formation. It can be used in topology and free-shape optimizations.
- *Extrusion constraint* allows to define a constant cross-section design for solid models in a specified direction, or along a curve. It can be used in topology and free-shape optimizations.
- *Grid constraints* can be set for free-shape optimization to limit grid's movement during process (along a plane, a vector or totally fixed).

Several manufacturing constraints can be combined at the same optimization process.

3.5 Convergence

It must be pointed out that even when constraints are settled up, OptiStruct has some margin to consider a feasible design. This means that slightly negative MOS can be obtained. In order to reach convergence, satisfaction of only one of the two tests used by OptiStruct is required.

- Regular convergence. For two consecutive iterations, the change in the objective function must be less than the objective tolerance and constraint violations must be less than 1%.
- Soft convergence. For two consecutive iterations, there is little or no change in the design variables.

3.6 OSSmooth

OSSmooth is a semi-automated design interpretation tool embed in HyperMesh, which facilitates recovery of a modified geometry resulted from a structural optimization for further use in the design process and FEA reanalysis.

OSSmooth can be used in three different ways: OSSmooth for geometry, FEA topology reanalysis, and FEA topography reanalysis.

OSSmooth (for geometry) is generally used to recover geometry by interpreting topology, topography, and shape optimization results. Resulting shapes can be smoothed.

Meanwhile, OSSmooth for FEA topology and FEA topography reanalysis are used to generate recovered geometry with boundary conditions for FEA reanalysis.

4 Structure description

The structure object of study is a habitable module designed to be part of a space station. It has two bulkhead-hatches in order to connect it to two other modules, being one of them an airlock. The primary structure of the module must fulfil the following mechanical requirements:

- Withstand loads during its whole life-time; i.e., testing, transportation, launch, on-orbit docking and on-orbit accelerations.
- Withstand internal ambient pressure and depressurization for emergency flight cases.
- Guarantee pressure containment.
- Withstand loads induced by the crew and secondary masses.
- Provide structural stiffness in accordance with dynamic requirements.

4.1 Components

The following components conform the module's primary structure:

- Axial cylinder,
- Top ring,
- Axial bulkhead,
- Axial hatch,
- Bottom ring,
- Access closure,
- Radial cylindrical segment,
- Radial ring,
- Airlock interface,
- Radial hatch,
- Longerons,
- Secondary masses.

In Figure 4.1, Figure 4.2, Figure 4.3, Figure 4.4, overall views of the module are provided. The Computer Aided Design (CAD) is property of Thales Alenia Space, therefore to safeguard confidentiality dimensions are not provided.

Axial cylinder

The axial cylinder corresponds to the habitable volume. Its baseline design consists of an unstiffened panel. However, it is divided by internal longerons to improve stiffness. It has a cylindrical shape to allow pressure loads to be smeared. The longerons are fastened to longitudinal ribs along the axial cylinder. Connection to the radial cylindrical segment and to the top and bottom rings is made by welding.

4. Structure description

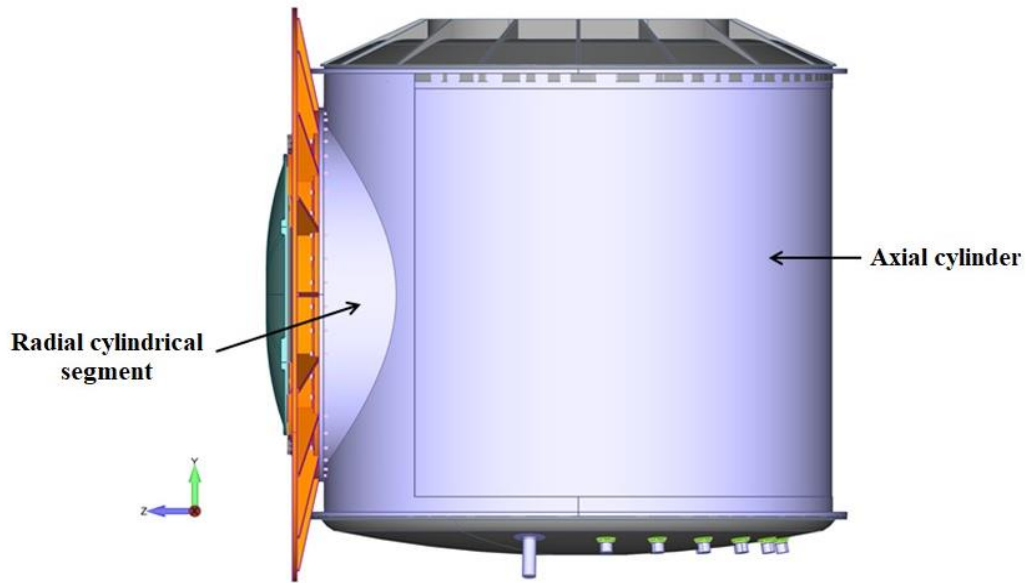


Figure 4.1. Lateral view of module's primary structure [1]

Top ring

The top ring connects the axial cylinder with the axial bulkhead. It is joined to the axial cylinder by means of a circular weld and bolted to the axial bulkhead.

Axial bulkhead

The axial bulkhead accommodates the docking mechanisms to allow connection with another module. It is bolted to the top ring.

Axial hatch

The axial hatch is mounted on the axial bulkhead. It permits crew, payload and equipment transfer when opened and guarantees pressure containment when closed.

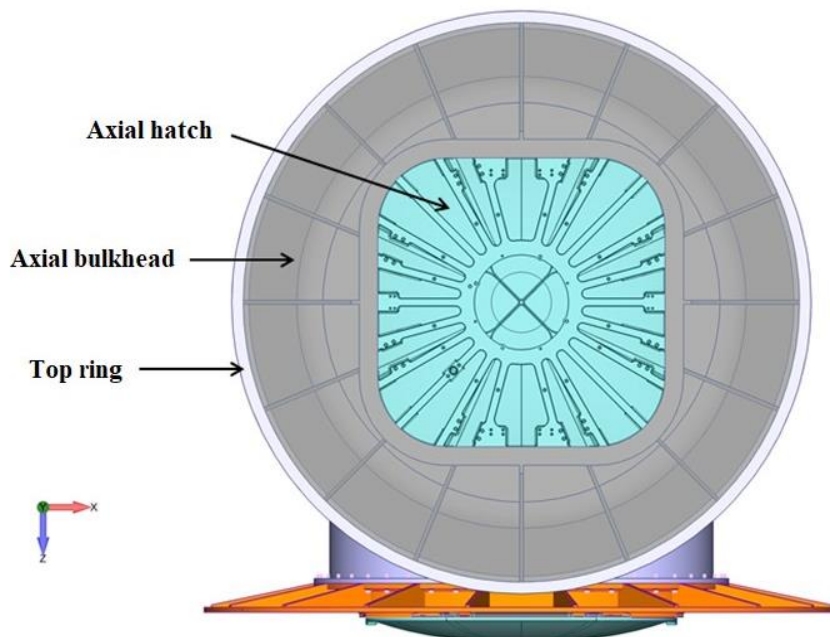


Figure 4.2. Top view of module's primary structure [1]

4. Structure description

Bottom ring

The bottom ring connects the axial cylinder with the access closure. It is joined to the axial cylinder by means of a circular weld and bolted to the access closure.

Access closure

The access closure is the bottom component of the module that encloses the habitable volume. It is fastened to the bottom ring.

Radial cylindrical segment

The radial cylindrical segment is the connection between axial cylinder and the airlock interface. It is welded to the axial cylinder and to the radial ring.

Radial ring

The radial ring connects the radial cylindrical segment with the airlock interface. It is joined to the radial cylindrical segment by means of a circular weld and bolted to the airlock interface.

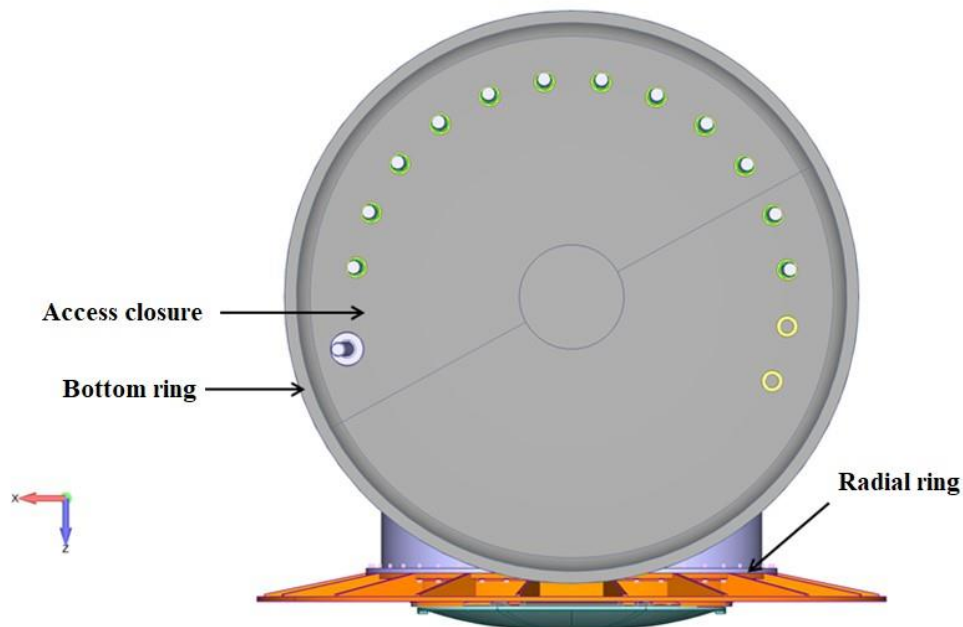


Figure 4.3. Bottom view of module's primary structure [1]

Airlock interface

The airlock interface accommodates the docking mechanisms and serves as interface with the airlock. It is bolted to the radial ring.

Radial hatch

The radial hatch is mounted on the airlock interface. It permits crew, payload and equipment access to airlock when opened and guarantees pressure containment when closed.

4. Structure description

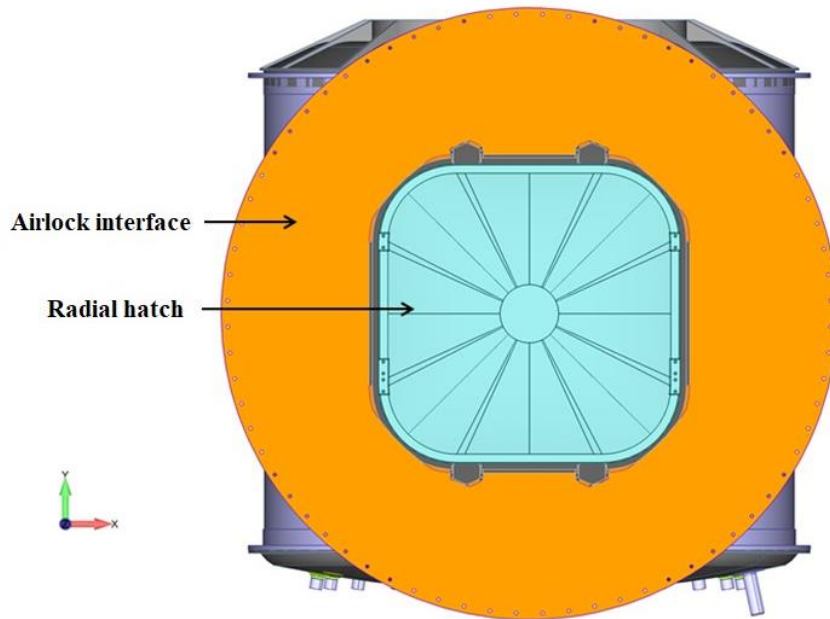


Figure 4.4. Front view of module's primary structure [1]

Longerons

Longerons are used to reinforce the axial cylinder in the longitudinal direction (see coordinate system in section 4.2) and transfer the loads induced by the secondary masses. They are fastened to the axial cylinder longitudinal ribs and connected to the top and bottom rings by means of an interface structure. Their location is indicated in Figure 4.6.

Secondary masses

Secondary masses include the payload, avionics, conditioning system and secondary structural components accommodated inside the axial cylinder. Payload typically includes supplies for the mission (i.e., water, food and spare parts) and small scientific experiments located inside of boxes. Meanwhile, conditioning system units (i.e., fluid pumps, power/data distribution units and ventilation fans) are usually located inside the racks.

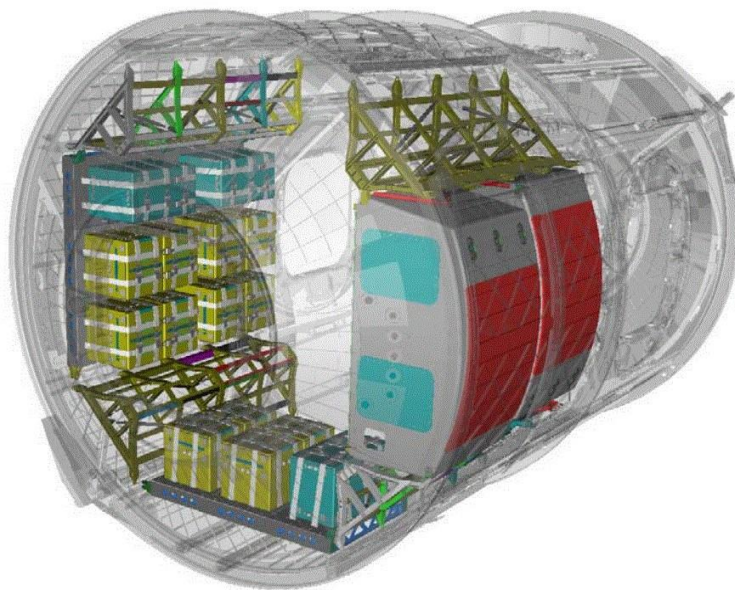


Figure 4.5. Example of secondary masses allocation [1]

4. Structure description

In Figure 4.5 there is an example of secondary masses allocation (coloured) inside the structure of a similar module. They consist of racks and boxes fixed to the primary structure (black and white) by means of secondary structural components attached to longerons and rings with brackets.

These secondary masses are estimated in 500 kg for the analysis driven in this work. Mass budget is divided equitably between three out of four-cylinder segments delimited by the longerons (see Figure 4.6). The segment in front of the airlock interface is not available. Each secondary mass fraction is considered fixed to the primary structure at rings and the longerons on their sides.

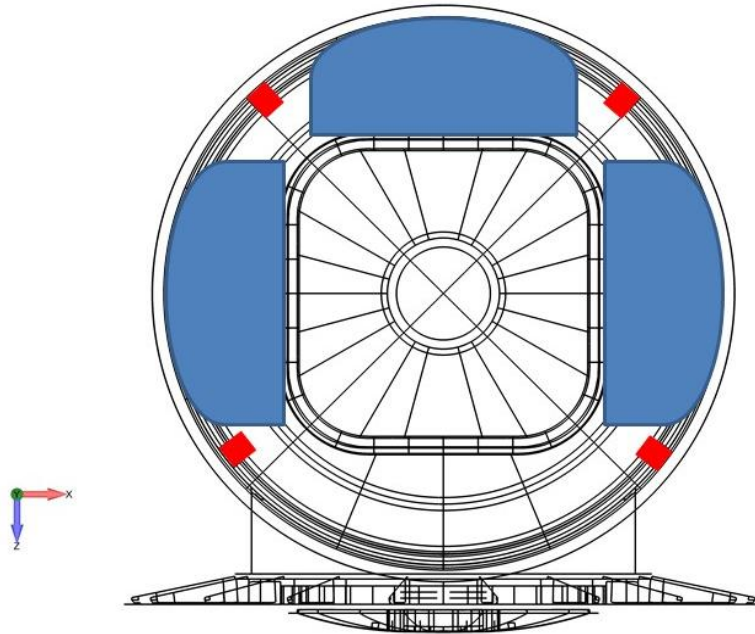


Figure 4.6. Schematic representation of secondary masses (in blue) between longerons (in red) [1]

4.2 Coordinate system

The module's coordinate system is the one displayed in Figure 4.7. Its origin is at the centre of the access closure. The Y axis is referred as the longitudinal direction. It is aligned with the axial cylinder and pointing to the axial hatch. The Z and X axis are the lateral directions as they are radial to the axial cylinder. The Z axis is pointing to the radial hatch, while X axis is perpendicular to the former one.

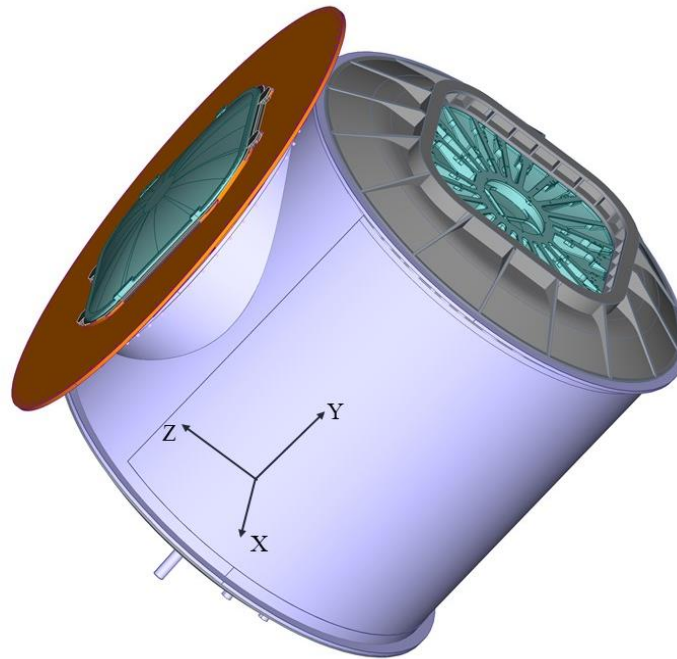


Figure 4.7. Module's coordinate system [1]

4.3 Material

The material chosen by Thales Alenia Space for the module's primary structure is Aluminium 2219-T851. Due to its mechanical properties (low density, but high mechanical performance) and low outgassing ratio, aluminium alloys are typical materials for structure components. Table 4.1 includes main material properties obtained in [8].

Modulus of elasticity in tension [MPa]	72395
Modulus of elasticity in compression [MPa]	74463.4
Poisson's ratio	0.33
Density [kg/m³]	2850
Thermal expansion coefficient [m/(m·K)]	$2.3 \cdot 10^{-5}$
Tensile yield allowable stress (F_{ty}) [MPa]	317.2

Table 4.1. Aluminium 2219-T851 properties

Aluminium 2219-T851 allowable stress for thin plates are provided by [8]. Although yield allowables were given for longitudinal and lateral grain directions, for the approach of the present work, we will consider an isotropic material. Therefore, most restrictive allowable stresses are chosen from both grain directions. For the same reason, tensile stress is chosen among tension and compression allowables.

4.4 Finite element model

The FE model of the structure was given by Thales Alenia Space as a result of a master thesis developed at Politecnico di Milano by Virtudes de Gregorio Roig [1].

Figure 4.8 shows in blue the mesh of the axial cylinder area which is object of optimization. All elements of this area of the mesh are CQUAD4 2D elements. They are associated to a PSHELL property modelling Aluminium 2219-T851 thin plates of different thicknesses. The elements in yellow correspond to the interface region in which longerons are attached to the cylinder panel.

4. Structure description

A complete description of the FE model with all the elements present can be found in Appendix A.

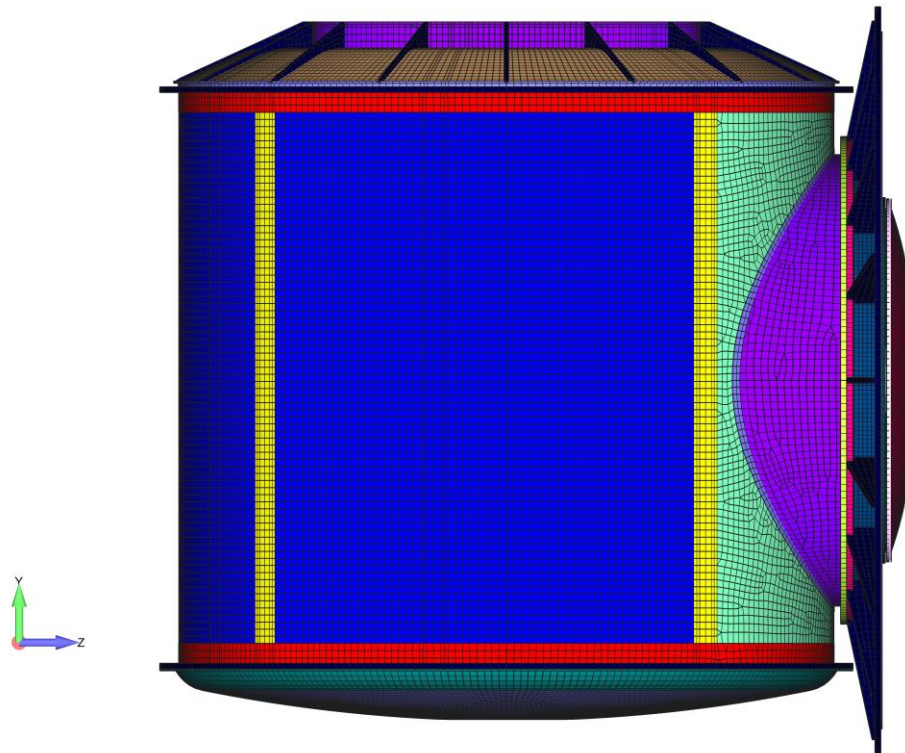


Figure 4.8. Lateral view of the FE model [1]

4.5 Constrains

As described in [9], it is supposed that the structure is cantilevered at the adapter interface during Ariane 5 launch. Constrains are applied to all degrees of freedom of 48 nodes as seen in Figure 4.9 marked by white circles.

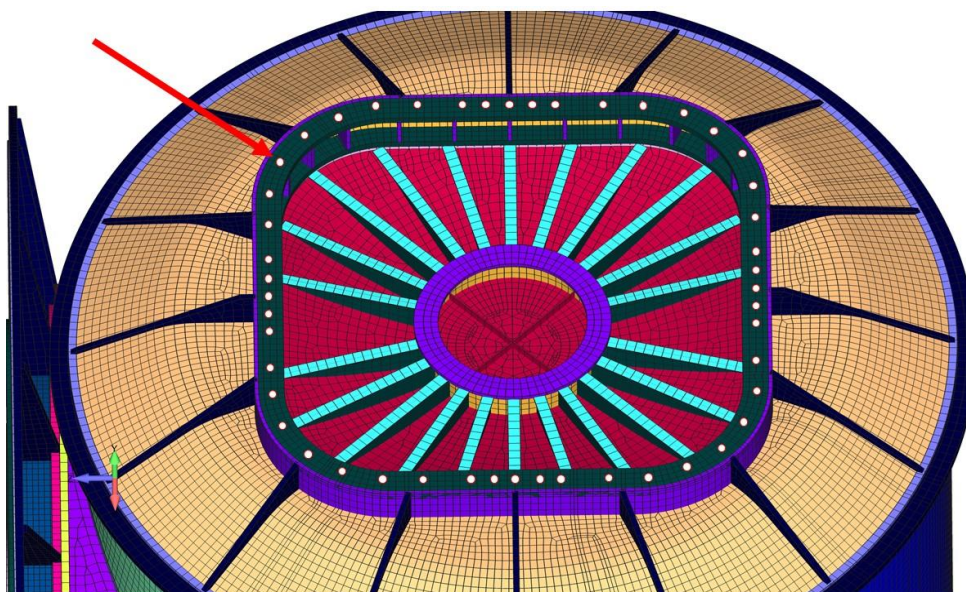


Figure 4.9. Constrained nodes [1]

5 Mechanical requirements and failure modes

Along this section, mechanical requirements to be fulfilled by the structure are exposed. For the scope of this work, failure modes to be checked are yield strength, axial cylinder global buckling and resonance. The requirements definition is done in accordance with [10] standards.

5.1 Limit Loads

The Limit Loads are the maximum loads a structure is expected to experience with a given probability, during the performance of specified missions in specified environments [10]. Even though these loads could be static or dynamic, only static accelerations and operative maximum pressure will be considered in the present work.

5.1.1 Quasi-Static Limit Loads

A quasi-static load is independent of time or it varies slowly, so that the dynamic response of the structure is not significant. The Quasi-Static Limit Loads correspond to the most restrictive combination of static and dynamic accelerations that can be encountered at any instant of the mission (ground and flight operations) [9]. For this purpose, it was supposed that Ariane 5 launcher would be used. Nevertheless, this optimization study can be adapted to any launcher.

The Quasi-Static Limit Loads for a spacecraft launched on Ariane 5 provided by [9] are shown in Table 5.1. They apply on the module's centre of gravity. Lateral loads may act in any direction simultaneously with longitudinal loads.

	Longitudinal	Lateral
Acceleration [g]	-2.5 / +6	+2

Table 5.1. Quasi-Static Limit Loads

Note that g corresponds to an acceleration of 9.81 m/s^2 and gravity load is included. The minus sign for longitudinal axis values indicates tension.

5.1.2 Pressure Limit Loads

The Pressure Limit Load is the maximum internal pressure that the module must withstand and it has a value of 104.8 kPa. It corresponds to the extreme environmental conditions for a pressurized payload in the International Space Station [11].

5.2 Panel stability

The stability (i.e. no buckling) of the structure shall be verified for the Design Limit Loads [10]. However, as the objective of this work is to develop a feasible design for the curved panels forming the primary structure of the module, only global buckling of these panels will be studied.

5.3 Primary modes

Spacecrafts launched on Ariane 5 must fulfil some requirements related to the primary modes associated with large effective masses [9]. The modal effective mass is a measure to classify the importance of a mode shape when a structure is excited by base acceleration (enforced acceleration). A high effective mass will lead to a high reaction force at the base, which must be avoided. Mode limitations depend on the relative orientation of the cantilevered spacecraft to the launcher and the total mass.

As a result, the fundamental frequency shall be $\geq 31 \text{ Hz}$ in the longitudinal axis and $\geq 9.5 \text{ Hz}$ in the lateral axis (see section 4.2 for coordinate system definition). Besides, no secondary modes

5. Mechanical requirements and failure modes

should be lower than the first primary mode. For this work, total mass of the module is supposed to be lower than 4500 kg.

5.4 Subcases

Regarding possible combinations of longitudinal and lateral quasi-static limit loads, 8 different subcases with different loads must be studied. X and Z refer to coordinate system directions in which lateral loads are applied, meanwhile Y coordinate system direction is the longitudinal axis as described in section 4.2. The ninth case corresponds to the internal pressure load acting on the inner faces of the module.

Subcase	Quasi-static loads [g]		
	X	Y	Z
1	2	-2.5	2
2	2	6	2
3	2	-2.5	-2
4	2	6	-2
5	-2	-2.5	2
6	-2	6	2
7	-2	-2.5	-2
8	-2	6	-2
9	Pressure load [Pa]		
	104800		

Table 5.2. Subcases

When defining the problem in OptiStruct, there will be a 10th subcase which will calculate the normal modes of the structure.

For all subcases, module's constraints are the ones defined in section 4.5.

5.5 Design Limit Loads

For determination of Design Limit Loads (DLL), Design Factor shall be used. It is defined as the product of the factors defined hereafter.

- A model factor $K_M = 1.2$ is applied to account for uncertainties in mathematical models when predicting dynamic response, loads and evaluating load paths.
- A project factor $K_P = 1.2$ is applied to account for the maturity of the program (e.g., stability of the mass budget, well identified design) and the confidence in the specification given to the project.

$$\text{Design Limit Loads} = \text{Limit Loads} \cdot K_M \cdot K_P \quad (5.1)$$

These factor values are based on relevant historical practice and recommended by [12].

Furthermore, different factors of safety are applied for each failure analysis. For the scope of this work, detrimental deformation and global buckling must be avoided. Therefore, the Design Yield Load and the Design Buckling Load are calculated by using a yield and a buckling factor of safety (FOSY, FOSB) as shown in the following equations.

$$\text{Design Yield Loads} = \text{Design Limit Loads} \cdot \text{FOSY} \quad (5.2)$$

$$\text{Design Buckling Loads} = \text{Design Limit Loads} \cdot \text{FOSB} \quad (5.3)$$

5. Mechanical requirements and failure modes

Factors of safety ensure a low probability of yielding or global buckling during loading at DLL level. Factors of safety for a metallic structural part of a pressurized manned module can be found in Table 5.3.

	FOSY	FOSB
Quasi-static loads	1.25	2
Internal pressure load	1.65	2

Table 5.3. Factors of safety

FOSY for the quasi-static cases are provided by [12], whereas they are provided by [13] for the internal pressure load. FOSB are obtained from [14].

5.6 Failure modes

Based on the mechanical requirements exposed, two failure modes will be determined by the use of margins of safety for yielding and buckling. A feasible design shall have all margins of safety positive. In [10], it is specified how to calculate the margins of safety. See Eq.(5.4).

$$MOS = \frac{\text{design allowable load}}{\text{design limit load} \cdot FOS} - 1 \quad (5.4)$$

As far as elastic behaviour is maintained, loads can be replaced by stresses in terms of design limits because the load- stress relationship is linear.

5.6.1 Yield strength

In order to determine yielding, the Maximum-Distortion-Energy or von Mises Criterion will be used. This criterion is based on the determination of the distortion energy in a given material, i.e., of the energy associated with changes in shape of that material. According to it, a given structural component is safe as long as the maximum value of the distortion energy per unit volume in that material remains smaller than the distortion energy per unit volume required to cause yield in a tensile-test specimen of the same material [15]. The margin of safety for this failure mode is calculated as,

$$MOS_{yield} = \frac{F_{ty}}{\sigma_{VM,max} \cdot K_M \cdot K_P \cdot FOSY} - 1 \quad (5.5)$$

where F_{ty} is the tensile yield strength and $\sigma_{VM,max}$ is the maximum value of the von Mises stress derived from the application of the Limit Loads. The values associated to design and safety factors for each subcase type can be found in section 5.4.

5.6.2 Global buckling of panel

OptiStruct solves linear buckling in finite element analysis by first applying a reference level of loading, f_{ref} , to the structure [4]. This reference load is the one present in each subcase from 1 to 8 as described in section 5.4. Buckling will not be calculated for the internal pressure subcase.

Afterwards, a linear static analysis is carried out to obtain stresses which are needed to form the geometric stiffness matrix K_σ , corresponding to f_{ref} . Buckling loads are then calculated by solving the eigenvalue problem expressed in Eq. (5.6):

$$(K - \lambda \cdot K_\sigma) \cdot A = 0 \quad (5.6)$$

5. Mechanical requirements and failure modes

where K , is the stiffness matrix of the structure and λ , the eigenvalue, is the multiplier to the reference load. The vector A is the eigenvector corresponding to the eigenvalue.

In order to solve the eigenvalue problem, a matrix method called the Lanczos method is used, where not all eigenvalues are required. Only a small number of the lowest eigenvalues are normally calculated for buckling analysis.

The lowest eigenvalue λ_α , also called the minimum buckling factor, is associated with buckling. The critical or buckling load is:

$$f_\alpha = \lambda_\alpha \cdot f_{ref} \quad (5.7)$$

A typical buckling constraint is a lower bound of 1.0 for the buckling factor, indicating that the structure is not to buckle with the given static load (f_{ref}). OptiStruct recommends to constrain the buckling factor for several of the lower modes, not just of the first mode. For the scope of this work first 5 modes will be checked.

Knock down factor

Experience has shown that large discrepancies often occur between theoretic shell stability analysis and its results from experiments. Empirical knock-down factors (KDF) are recommended by buckling design guidelines, like [14] and [16]. They are intended to compensate those differences mainly caused by geometrical imperfections, residual stresses and pre-buckling deformations.

NASA SP-8007 [16] is a widely used reference for computing knock-down factors for cylindrical thin walls, depending on the radius cylinder (R) and wall thickness (t) ratio. They are calculated following Eq. (5.8)

$$\gamma = 1 - 0.901_\alpha \cdot (1 - e^{-\phi}) \quad (5.8)$$

where,

$$\phi = \frac{1}{16} \cdot \sqrt{\frac{R}{t}} \quad \text{for } \frac{R}{t} < 1500 \quad (5.9)$$

If the knock-down factor is multiplied by the buckling load, then it is obtained a lower bound for considered experimental data. That is the reason why this function is part of the Lower Bound Design Philosophy [14].

Even though [14] considers [16] functions conservative, this method does not require knowledge about pattern or even amplitude of imperfection, which are very costly to measure and introduce in analyses. Besides, it must be considered that knock-down factors in [16] correspond to complete cylinder panels, while the case of study is a cylinder covering only 79° of circumference. However, as part of a preliminary design of the structure and to check OptiStruct capabilities, method suggested in [16] is sufficient.

It possible to multiply that 1 by the knock down factor, which varies with thickness.

Finally, if knock-down factor is multiplied by the buckling load, according to Eq. (5.4), the margin of safety is computed using the following equations:

$$MOS_{buck} = \frac{\gamma \cdot f_{\alpha}}{f_{ref} \cdot K_M \cdot K_P \cdot FOSE} - 1 = \frac{\gamma \cdot \lambda_{\alpha}}{K_M \cdot K_P \cdot FOSE} - 1 \quad (5.10)$$

5.6.3 Primary modes

As far as the fundamental frequencies of the panel/module are higher than the limits established for longitudinal and lateral axis in section 5.3 taking into account the effective mass associated, failure will be avoided

6 Preliminary analyses

In the present chapter, a preliminary analysis is performed to the structure before the axial cylinder optimization takes place. Results obtained will be compared with those resulting from optimization.

In order to safeguard confidentiality, lengths are given in non-dimensional form obtained by dividing by an arbitrary length. As a result, the non-dimensional baseline thickness of the axial cylinder panels before optimization is set to 1 N.d. (non-dimensional).

6.1 Analysis set up

Area of study

As the objective of this chapter is to obtain some preliminary results in order to compare them with the optimization solution, the area of study for the preliminary analyses is the same as for the optimization.

The purpose of this work is to check OptiStruct capabilities to optimize the axial cylinder structure of a generic space module. However, the area of study is limited to the one coloured in blue in Figure 6.1. The area near to the bottom and top rings is not included because stresses depend on the welding technology used to connect the axial cylinder to the rings. Therefore, this area must be studied separately, which is not scope of this work.

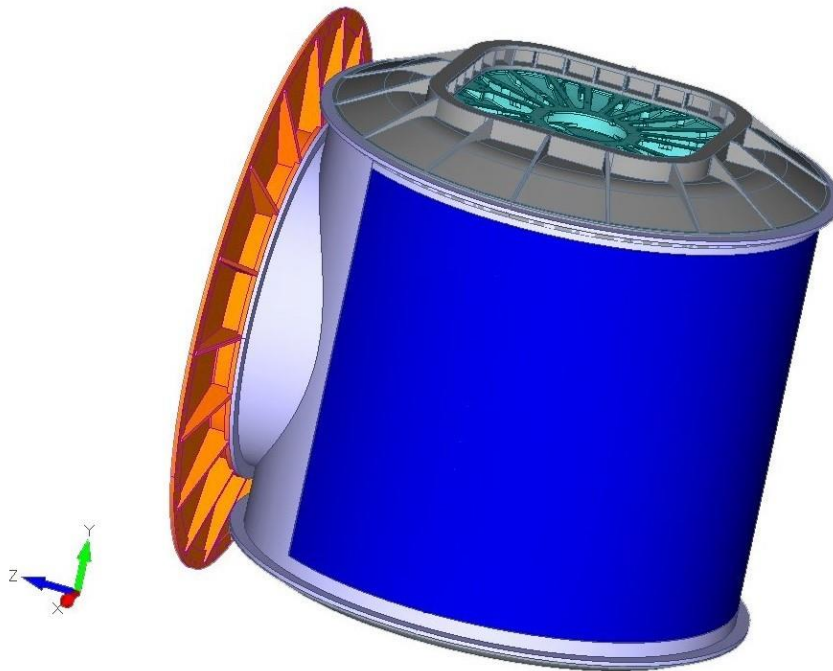


Figure 6.1. Module's area of study [1]

Subcases

The list of subcases studied is the one described in section 5.4 with model constrained as specified in section 4.5.

Failure modes

Yield strength and global buckling will be checked for the axial cylinder area. In addition, resonant frequencies will be determined for the whole module. The failure modes will be determined as described in section 5.6.

6. Preliminary analyses

It is recalled that FOSY has different values for quasi-static (subcases 1-8) and pressure loads (subcase 9).

6.2 Results

Results of total mass, maximum von Mises stresses, minimum buckling factors and computed margins of safety are summarized in Table 6.1.

	Quasi-static loads (subcases 1-8)	
	Yield Strength	Limiting subcase
$\sigma_{VM,max}$ [MPa]		18.56
MOS_{yield}		8.50
Pressure loads (subcase 9)		
$\sigma_{VM,max}$ [MPa]		62.95
MOS_{yield}		1.12
Global Panel Buckling	Limiting subcase	2
	λ_α	28.59
	KDF	0.32
	MOS_{buck}	2.18

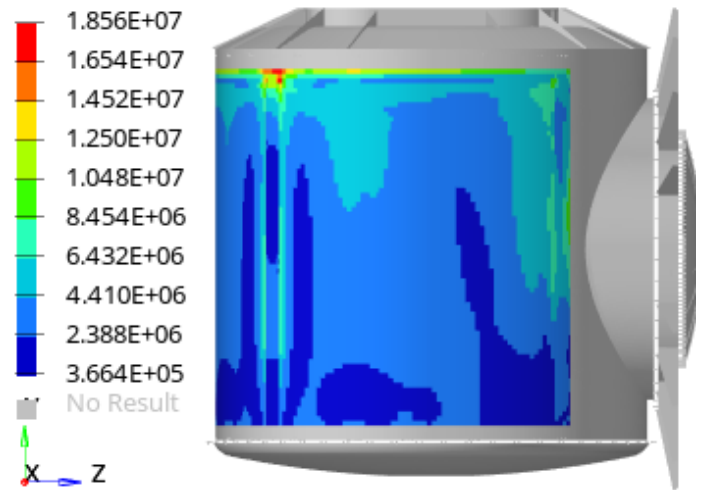
Table 6.1. Preliminary stress and buckling results

As it can be seen from results, all MOS are higher than 0. This means that axial cylinder with 1 N.d. thickness is a feasible design as it fulfils all mechanical requirements established. However, it can also be concluded that total mass of the module (977.41 kg) can be minimized by decreasing thickness of the curved panels. Thus, optimization of thickness can be applied.

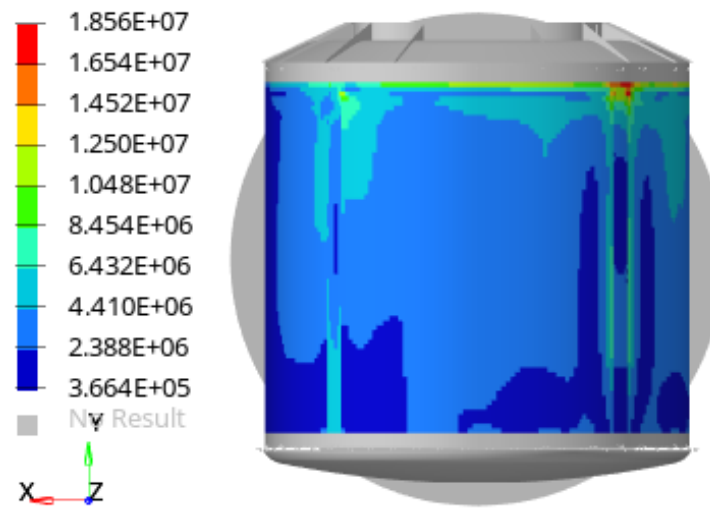
In Figure 6.2 the enveloped distribution of maximum von Mises stresses for subcase 8, which presents the highest values, can be found. However, it is remarkable that subcases 2, 4 and 6 obtained similar results as all of them correspond to compression loads in the axial cylinder, which are higher than tension loads. Maximum values of von Mises stress are located at the top edge of the axial cylinder, close to the union with the top ring. Besides, stresses increase near longerons attachments.

Figure 6.3 reports von Mises results for the internal pressure loads (subcase 9). In this case, maximum values are obtained in the lateral extremes of the axial cylinder. This is caused by the vicinity of the radial segment union, which causes a discontinuity in the mesh. However, performance will improve in the real structure as there will be a fillet.

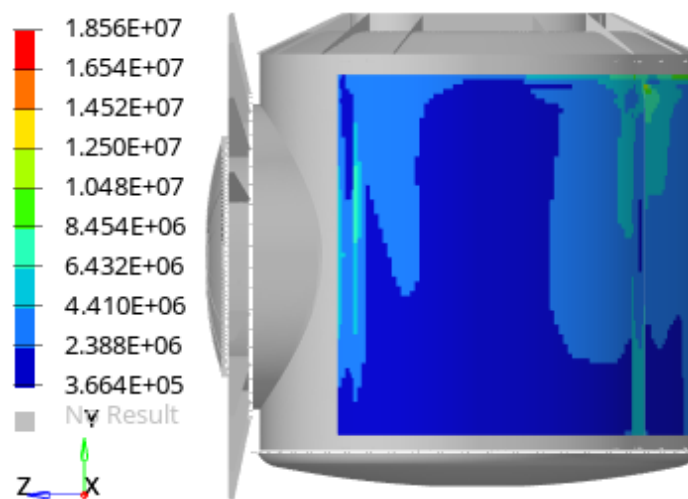
6. Preliminary analyses



(a) Left view



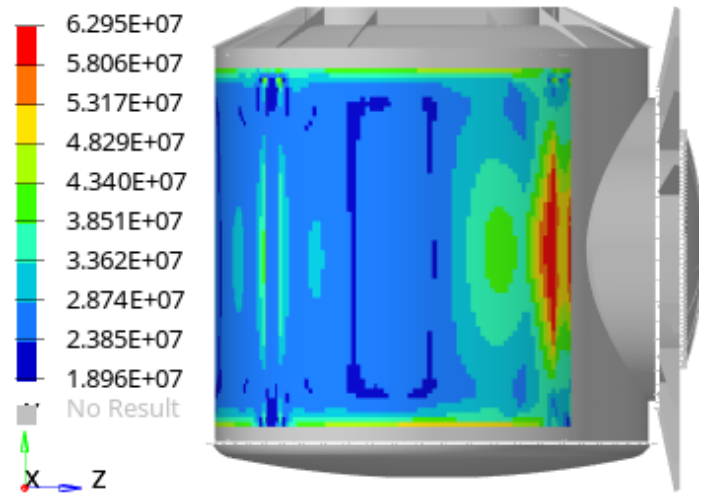
(b) Back view



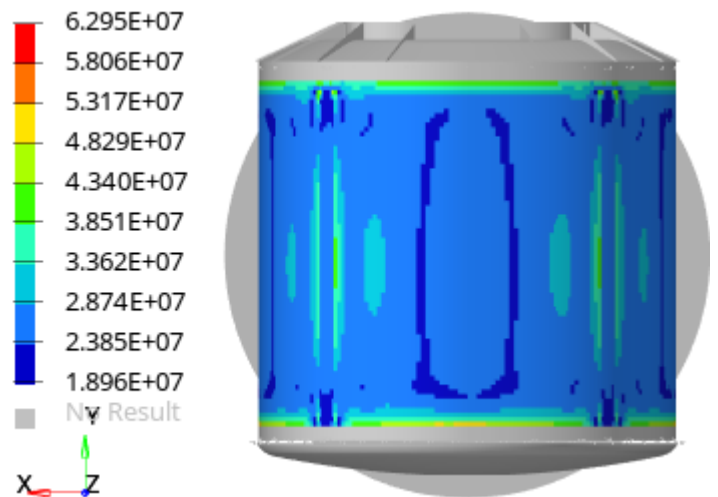
(c) Right view

Figure 6.2. Maximum von Mises stresses [Pa] for quasi-static loads (subcase 8)

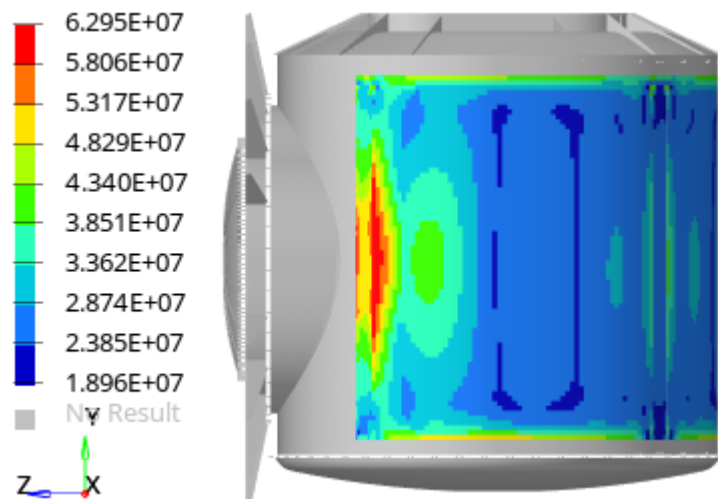
6. Preliminary analyses



(a) Left view



(b) Back view



(c) Right view

Figure 6.3. Maximum von Mises stresses [Pa] for pressure loads (subcase 9)

6. Preliminary analyses

Related to buckling results, the subcase with the minimum buckling factor is the subcase 2. Corresponding buckling shape can be seen in Figure 6.4.

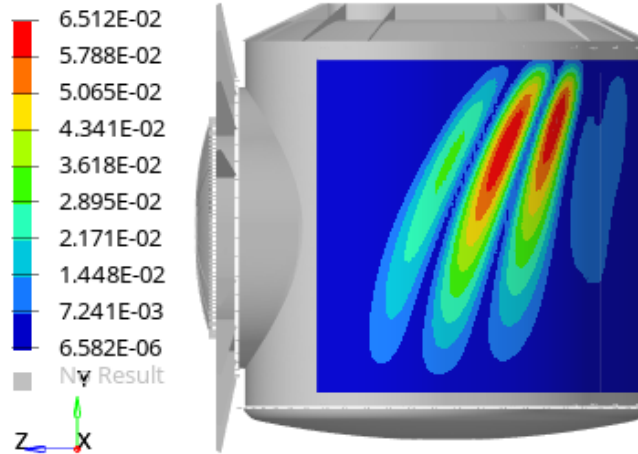


Figure 6.4. Buckling shape for subcase 2 with displacement contour (m)

Table 6.2 gives a list of frequencies and mass fractions for the first 15 normal modes of the module structure. The modal effective mass fraction of each mode indicates how much of the total mass is represented by that mode, therefore the maximum effective mass values will be associated to the primary modes for each direction.

Results show that the primary mode in the longitudinal direction (Y-Trans) is the fourth mode with an effective mass fraction equal to 81%. On the other hand, primary modes for the lateral directions, X-Trans and Z-Trans, are the first and the second modes with a 65% and 64% of effective mass, respectively. When compared with minimum frequencies requirements established by Ariane 5 launcher, both are fulfilled: the first longitudinal mode's frequency is 49.64 Hz, which is higher than 31 Hz; and the first lateral mode's frequency is 17.47 Hz, which is higher than 9.5 Hz.

Mode	Frequency [Hz]	X-Trans [%]	Y-Trans [%]	Z-Trans [%]	X-Rot [%]	Y-Rot [%]	Z-Rot [%]
1	17.47	65	0	0	0	3	12
2	19.01	0	0	64	14	5	0
3	43.89	1	0	0	0	34	1
4	49.64	0	81	1	1	0	3
5	54.63	0	9	2	1	0	0
6	59.08	0	0	0	0	3	0
7	65.67	0	3	2	3	0	0
8	66.35	5	0	0	0	2	5
9	79.31	0	0	3	2	0	0
10	86.39	2	0	0	0	20	2
11	88.53	0	1	9	5	1	0
12	96.86	0	0	0	0	0	0
13	97.50	1	0	0	0	3	0
14	102.2	0	0	1	0	0	0
15	103.9	0	0	0	0	4	0

Table 6.2. Modal preliminary analysis results

6. Preliminary analyses

In Figure 6.5, Figure 6.6, Figure 6.7, modal shapes corresponding to the primary lateral and longitudinal modes, respectively, are shown.

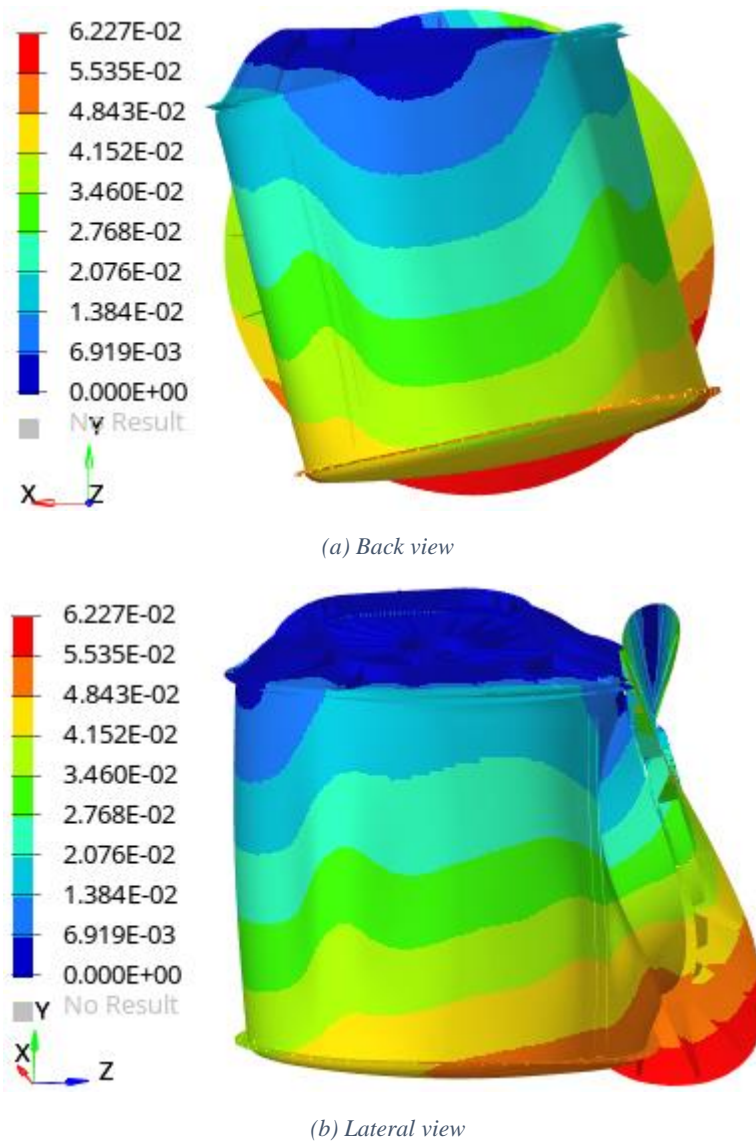


Figure 6.5. Mode 1 (first lateral mode) deformed representation ($\times 10$) and mass normalized displacement contour (m)

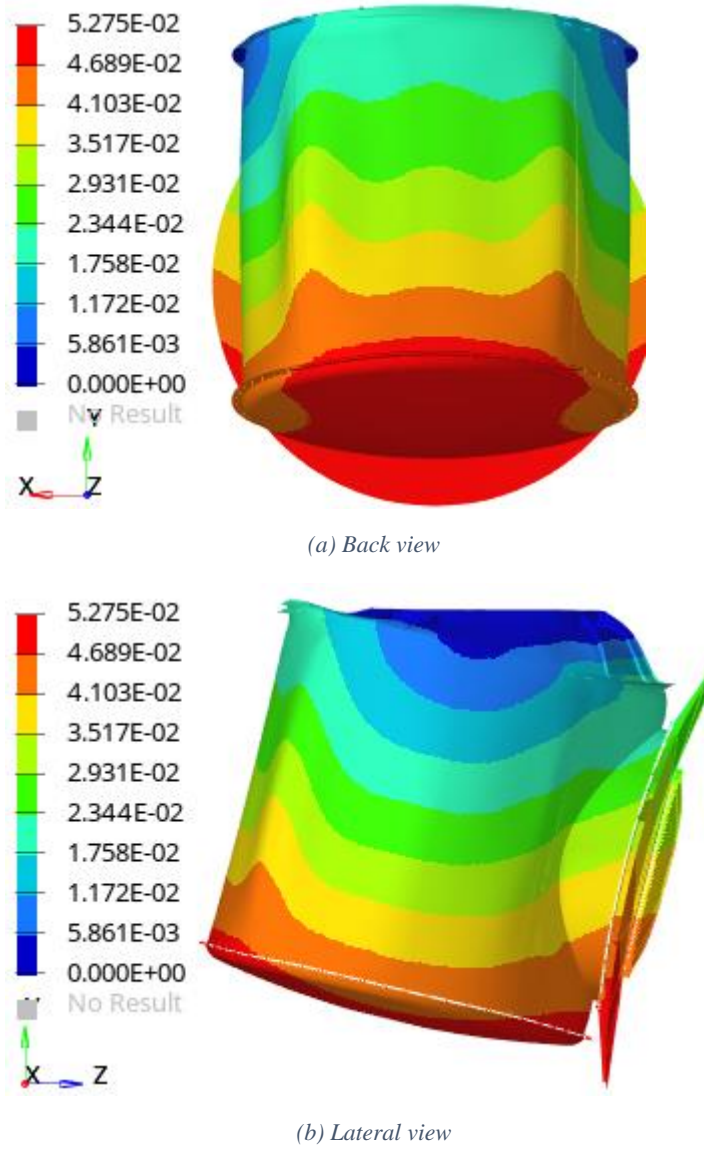


Figure 6.6. Mode 2 (second lateral mode) deformed representation ($\times 10$) and mass normalized displacement contour (m)

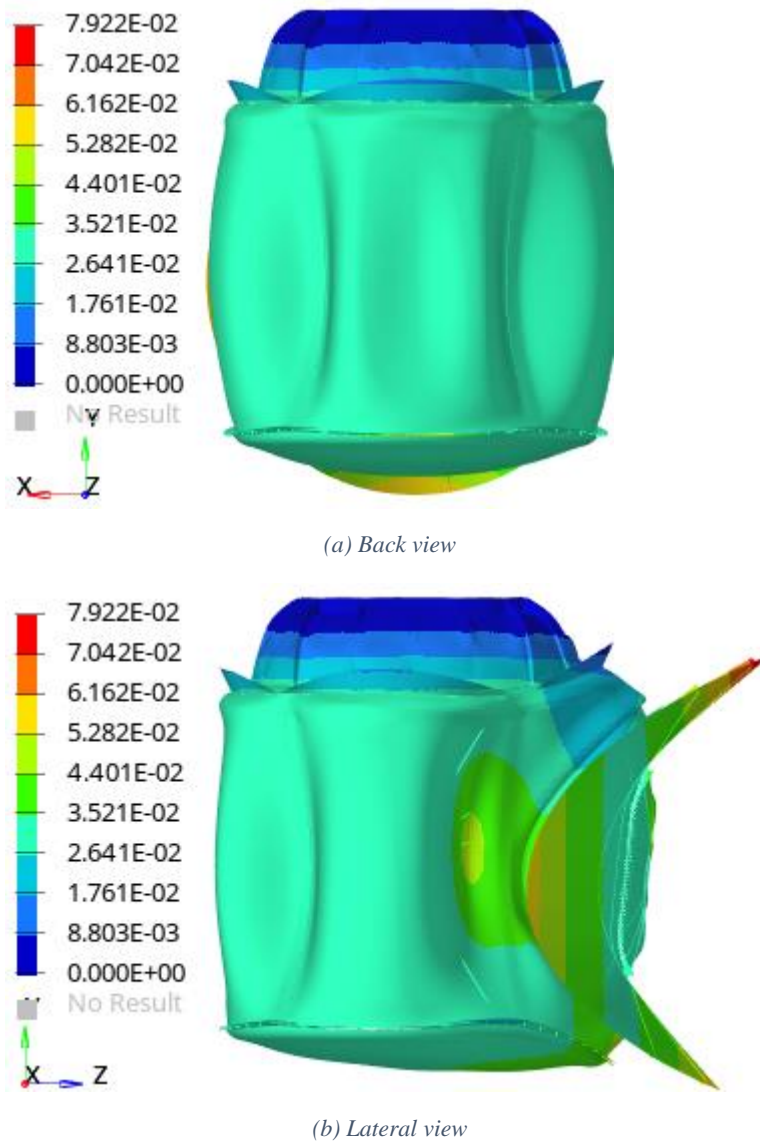


Figure 6.7. Mode 4 (first longitudinal mode) deformed representation ($\times 10$) and mass normalized displacement contour (m)

In general, results that can be compared to the ones obtained in Virtudes de Gregorio work [1] for the same preliminary analysis, are coincident. Only small differences can be observed, probably due to the different FE solver used: OptiStruct vs Nastran.

7 Optimization of an unstiffened curved panel

In the present chapter, optimization of the panel thickness for the curved panel of the axial cylinder is developed and compared with results obtained in the preliminary analyses and in Virtudes de Gregorio master thesis [1]. For this process, free-size optimization will be performed.

7.1 Optimization set up

Optimization model

As described in section 6.1, the optimization model corresponds to the main area of the axial cylinder, which is divided in four segments by the longerons; three of them are curved panels and in the fourth one the radial segment connection is located. The curved segments represent the main area of the axial cylinder which is object of study.

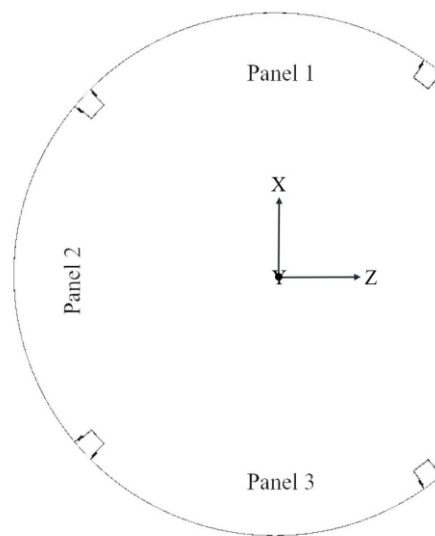


Figure 7.1. Optimization model [1]

Subcases

The list of subcases studied is the one described in section 5.4 with model constrained as specified in section 4.5.

Objective

The objective of the optimization is to minimize the total mass of the module, which depends on the panel shell thickness. Thus, a mass response must be defined in OptiStruct.

Design variables

For a free-size optimization, the design variables correspond to thickness of each shell element included in the optimization model. For maximum thickness, 1 N.d. will be chosen as it was already checked that this value is enough to fulfil mechanical requirements. 0.143 N.d. will be set as minimum thickness for manufacturing reasons.

It is important to set a pattern group manufacturing constraint for uniform thickness for the whole optimization model. In other case, different thickness values will be obtained for each element.

Constraints

7. Optimization of an unstiffened curved panel

In order to check yield strength and global buckling failure modes, two responses will be defined: one for von Mises static stress and another one for buckling. To introduce maximum and minimum constraints, it is necessary to calculate values for which each response will have at least $MOS = 0$. It is recalled that FOSY has different values for quasi-static (subcases 1-8) and pressure loads (subcase 9). Taking into account FOS, design factors and KDF, limit values for these responses are:

- For von Mises constraint, upper boundaries are 176.22 MPa for subcases 1-8 and 133.50 MPa for subcase 9. If stresses go higher than these values, yielding will occur.
- For buckling constraint, lower boundary is 9.80. OptiStruct does not have the option to update the KDF with each iteration, therefore an initial value is supposed (0.857 N.d.) based on optimized thickness resulted for the same module obtained by Virtudes de Gregorio [1], which corresponds to a KDF equal to 0.294.

If optimized thickness is not the same as the one obtained in [1], optimization will be repeated with the updated KDF.

7.2 Results

After three iterations updating the KDF based on the thickness, the final optimized shell thickness got **0.643 N.d.** The final KDF used corresponds to previous iteration with a value of 0.256. This iterative process stopped when values were differing less than 0.05 mm.

Optimized total mass corresponds to 955.57 kg. It means that 21.84 kg (2.23% of primary structure mass) can be saved by minimizing panel thickness for the optimization area.

Each optimization process took around 51 minutes of computing time.

Buckling analyses

Buckling is the controlling failure mode, i.e., the one that gives lower MOS. The most critical load cases correspond to the compression loads in the longitudinal axis which are larger than the tension ones; the subcase 2 (2g X, 6g Y, 2g Z) and the subcase 6 (-2g X, 6g Y, 2g Z).

In Table 7.1 results for the buckling analysis are shown. As it was mentioned, buckling was the controlling failure mode during optimization, therefore its MOS reaches zero; which is the limit imposed for avoiding buckling taking into account FOS, KDF and design factors. When compared with previous values obtained for the baseline model, it can be seen that the limiting subcase is still the same, but MOS is reduced to the extreme.

	Optimized model	Baseline model
Limiting subcase	2	2
λ_α	11.25	28.59
KDF	0.256	0.32
MOS_{buck}	0	2.18

Table 7.1. Buckling analysis results for optimized and baseline models

See Figure 7.2 for the optimized buckling shape. In general, buckling shapes are similar to the ones obtained in the preliminary analysis (Figure 6.4).

7. Optimization of an unstiffened curved panel

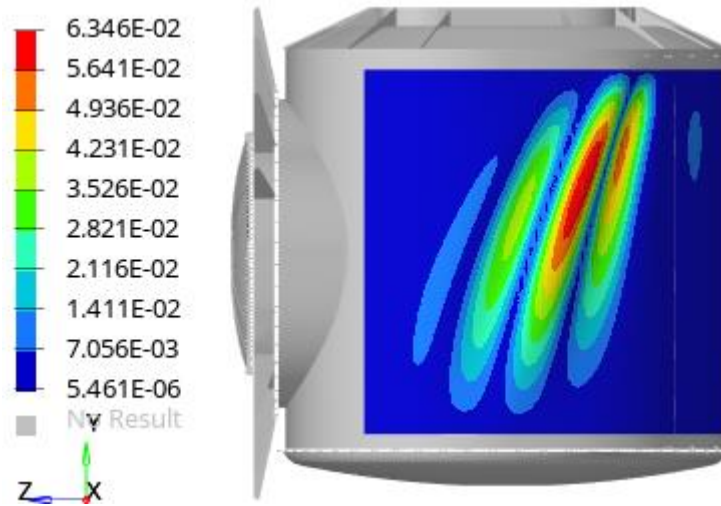


Figure 7.2. Buckling shape for subcase 2 after optimization with displacement contour (m)

Yield strength analysis

As thickness has decreased, von Mises stresses after optimization are higher. Nevertheless, the most critical subcase, the lowest MOS, corresponds to the internal pressure loading (load case 9) as it occurred for baseline model. Consequently, Table 7.2 shows that MOS has decreased up to a closer-to-zero value, but not until the minimum value as it happened with the buckling failure mode.

With respect to the quasi-static load cases (subcase 1-8), the one with lowest MOS is the 8th one. It is the same solution as for the baseline analysis.

	Optimized module									Baseline module
Subcase	1	2	3	4	5	6	7	8	9	9
$\sigma_{VM,max}$ [MPa]	18.72	19.15	13.93	24.58	18.40	19.21	13.92	24.96	74.19	62.95
MOS_{yield}	8.41	8.20	11.65	6.17	8.58	8.17	11.66	6.06	0.80	1.12

Table 7.2. Yield strength analysis results for optimized and baseline models

Although, von Mises stress magnitudes have increased, location of maximum stresses are similar to the ones obtained in the preliminary analysis as it can be seen in Figure 7.3.

7. Optimization of an unstiffened curved panel

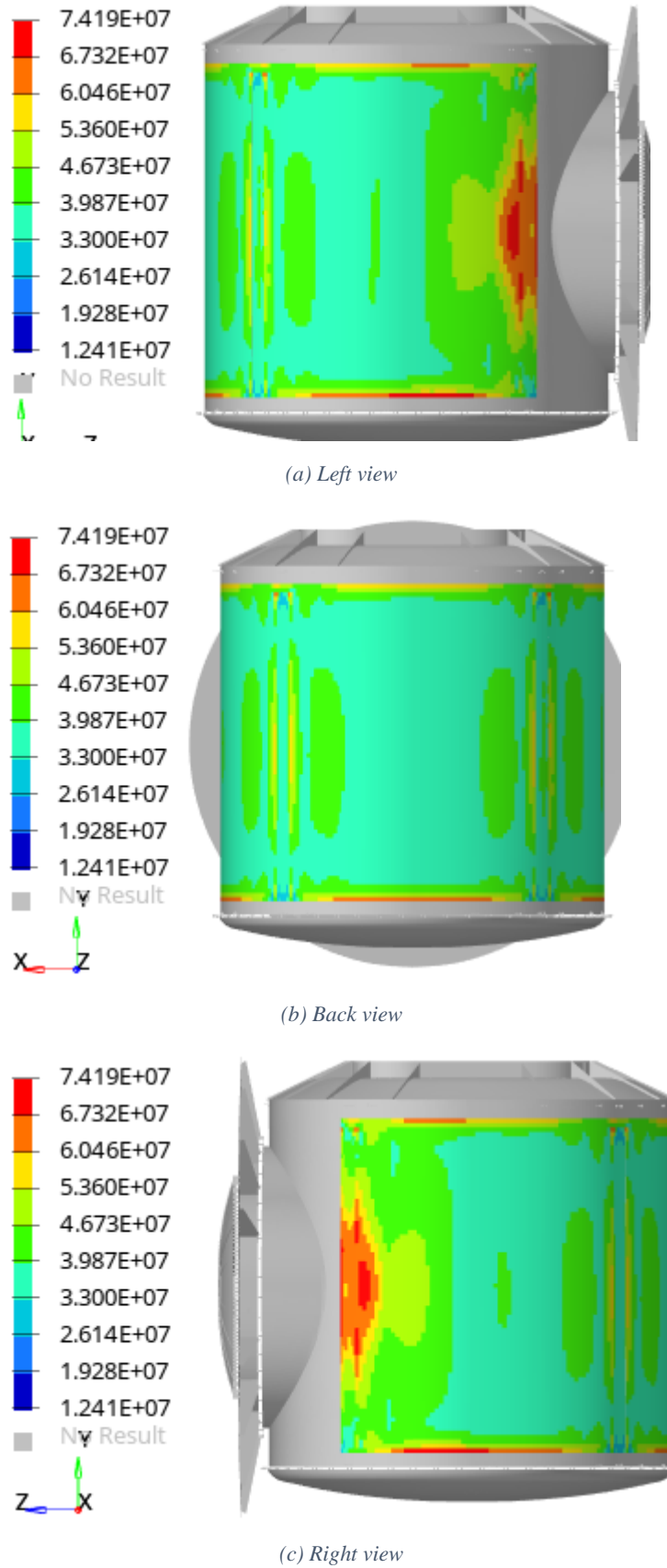


Figure 7.3. Maximum von Mises stress [Pa] after optimization for pressure loads (subcase 9)

7.3 Normal modes analysis

Normal modes were not introduced in the optimization process as a constraint because then computing time would have been increased considerably. Whereas, a simple modal modes analysis was carried out with the final thickness shell for the optimization model.

A list of frequencies and mass fractions for the first 15 normal modes of the module structure is displayed in Table 7.3. In this case, the longitudinal direction (Y-Trans) has its primary mode in the fourth mode with an effective mass fraction equal to 81%. Meanwhile, primary modes for the lateral directions, X-Trans and Z-Trans, are the first and the second modes with a 65% of effective mass in both cases. Requirements established by Ariane 5 launcher are fulfilled: the first longitudinal mode's frequency is 48.27 Hz, which is higher than 31 Hz; and the first lateral mode's frequency is 17.49 Hz, which is higher than 9.5 Hz.

Mode	Frequency [Hz]	X-Trans [%]	Y-Trans [%]	Z-Trans [%]	X-Rot [%]	Y-Rot [%]	Z-Rot [%]
1	17.49	65	0	0	0	3	12
2	19.01	0	0	65	13	5	0
3	42.66	1	0	0	0	39	1
4	48.27	0	81	0	0	0	3
5	52.02	1	0	0	0	0	0
6	59.98	5	0	0	0	1	1
7	63.08	0	5	1	2	0	0
8	76.40	0	0	2	2	0	0
9	78.16	1	0	0	0	12	1
10	80.14	0	1	6	4	0	0
11	84.15	1	0	0	0	1	1
12	86.02	0	1	3	2	0	0
13	87.48	0	0	0	0	0	0
14	87.89	0	0	0	0	5	0
15	89.41	1	0	0	0	3	0

Table 7.3. Modal analysis results for optimized module

These results can be compared to the analogous ones obtained for the baseline model in Table 6.2. For this purpose, Table 7.4 has been created in order to compare primary frequencies and effective mass ratios by showing difference between the optimized and the preliminary results.

In the primary modes there are almost no changes on frequencies nor effective masses. However, with larger modes, differences arise, especially in the frequency values. Nevertheless, these variations are far from the zone of interest: the first mode for each direction.

7. Optimization of an unstiffened curved panel

Mode	Frequency [Hz]	X-Trans [%]	Y-Trans [%]	Z-Trans [%]	X-Rot [%]	Y-Rot [%]	Z-Rot [%]
1	-0,02	0	0	0	0	0	0
2	0	0	0	-1	1	0	0
3	1,23	0	0	0	0	-5	0
4	1,37	0	0	1	1	0	0
5	2,61	-1	9	2	1	0	0
6	-0,9	-5	0	0	0	2	-1
7	2,59	0	-2	1	1	0	0
8	-10,05	5	0	-2	-2	2	5
9	1,15	-1	0	3	2	-12	-1
10	6,25	2	-1	-6	-4	20	2
11	4,38	-1	1	9	5	0	-1
12	10,84	0	-1	-3	-2	0	0
13	10,02	1	0	0	0	3	0
14	14,31	0	0	1	0	-5	0
15	14,49	-1	0	0	0	1	0

Table 7.4. Modal analysis difference results. Values refer to difference between optimized model minus baseline results

Mode shapes and total translation contour have no notable differences with respect to the baseline results.

7.4 Comparison of optimization results with HyperSizer

Optimization of the same axial cylinder panel thickness was done in [1] by Virtudes de Gregorio by using Nastran as solver and HyperSizer as optimization tool. Same load cases were employed. In order to extract FEA results from Nastran, different methods were used to condensate them and proceed with optimization in HyperSizer. In this way, computing time could be reduced. From the methods used, the Element-Based method considers all FEA shell element forces combination, so it is equivalent to consider all FEA results without condensation as it is the case of the present work. Therefore, results comparison must be done taking into account this method. However, an assumption was made in Virtudes de Gregorio work to reduce computing time: FEA loads are assumed constant along iterations. This means that final design variables chosen as the optimized candidate could be different from the real optimum design.

In [1], in spite of working with the complete FE model, optimization model was divided into 3 panels and they were studied separately as this way the only computationally allowable way to determine optimized structure with HyperSizer.

Even though exact results are expected, resulting optimized thickness is slightly different; 0.857 N.d. vs 0.643 N.d. This is probably due to the fact that in [1], a discrete design variable was set for the panel thickness with an increment of 0.143 N.d. Whereas, OptiStruct allows user to choose between a continuous variable when using free-size optimization, or a discrete variable for sizing optimization.

In both works, buckling is the controlling failure mode and the critical subcases correspond to the maximum compression loading. However, minimum MOS for buckling analysis obtained in [1]

7. Optimization of an unstiffened curved panel

did not reach zero as in the present work. Results obtained by Virtudes de Gregorio are shown in Table 7.5.

Element-Based method		
Component	Controlling load case	Minimum buckling MOS
Panel 1	4	0.35
Panel 2	4	0.36
Panel 3	8	0.35

Table 7.5. Buckling analysis results obtained in [1] (Table 5.6)

Differences in results may be due to the fact that continuous design variable is not available, hence limit design cannot be reached. In addition, different buckling calculation methods are used by each solver. Furthermore, HyperSizer is able to update KDF value for each optimization iteration, but even though KDF calculation done by HyperSizer is supposed to follow the function suggested in [16], as it was done in the present work, not the same results are obtained for these factors (0.4 vs 0.256).

Related to strength analysis, both works conclude that the internal pressure loads are the most critical from static loading subcases. The minimum MOS obtained in the present work (MOS equal to 0.80) does not considerably differ from the ones obtained in [1], which can be observed in Table 7.6. As buckling is the controlling failure mode to determine shell thickness, this lower value may be due to the variation in the final panel thickness. The lower the thickness, the higher the stresses, so the lower the MOS. Nevertheless, another difference is found in the strength analysis calculations. In the present work, only yielding failure is checked by following the Maximum-Distortion-Energy theory. On the contrary, in [1], apart from yielding, ultimate strength is also checked, both for tension and compression in the different shell directions. Despite of these variations, they do not affect optimized thickness result as strength analysis is not the controlling failure mode in any of the works.

Element-Based method		
Component	Controlling failure mode	Minimum strength MOS
Panel 1	Isotropic Strength, Yield, Longitudinal Direction	0.943
Panel 2	Isotropic Strength, Yield, Transverse Direction	1.363
Panel 3	Isotropic Strength, Yield, Longitudinal Direction	0.933

Table 7.6. Strength analysis results obtained in [1]

8 Optimization of a reinforced curved panel

In this chapter, different optimizations will be held in a single curved panel in order to check OptiStruct capabilities, instead of in the complete module as it was done before. This way, it is possible to conclude whether an optimization type could be useful to output a stiffened curved panel design.

When performing any optimization type on the simple curved panel model following the original constraints established in section 5.6, yield strength failure becomes the controlling failure mode. On the contrary, in the complete model optimization studied in the previous chapter, buckling was the most critical response. This is due to the fact that the curved panel with the constraints and loads imposed is not representative of the complete space module.

Stiffeners are really useful to improve buckling structure performance. However, they do not contribute in the same way to stress results. Hence, buckling constraints will be hardened with respect to the original ones declared in section 5.6, in order to optimize a curved panel where buckling failure is the controlling mode. In this way, a pattern of stiffeners that contribute to prevent buckling can be obtained, as it is desired for the panels forming the axial cylinder of the complete space module.

Buckling constraint will be set to the lower boundary that allows buckling to be the controlling failure mode in a similar way as it was for the complete space module optimization. After several iterations, the lower boundary for buckling factor that corresponds to these criteria is set to 65.

8.1 Optimization model

The axial cylinder is divided into four segments by the longerons; three of them are curved panels and in the fourth one the radial segment connection is located (see Figure 7.1). Those three panels have identical dimensions and must use same cross-section and material. Thus, one single panel model will be used for the optimization process, even though they do not have the same transmitted loads. In consequence, a simpler iterative process will be held in terms of computing time. This approach is valid in order to obtain a preliminary design of the stiffened panels of the axial cylinder.

In Figure 8.1, main dimensions for the panel under study are shown. The long span (a) is parallel to Y direction of the module coordinate system (see section 4.2), measuring 428.58 N.d. The curved span (b) has an arch of 354.29 N.d. and a radius of curvature (R) equal to 257.14 N.d.

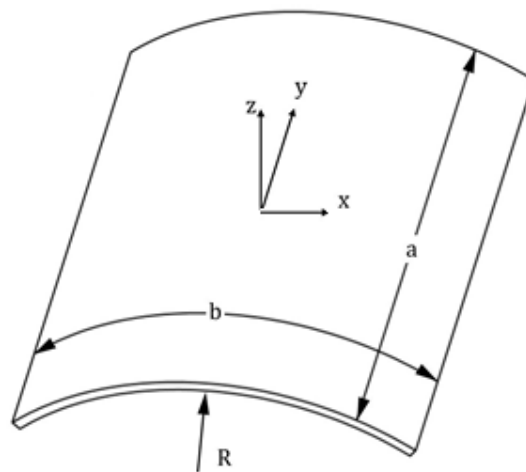


Figure 8.1. Panel dimensions

8. Optimization of a reinforced curved panel

A local coordinate system is defined in the panel segment. The x and y axis lie in panel lowest-surface. The z axis goes in the radial direction, the y axis is parallel to the straight span (a), so it coincides with the longitudinal direction of the module (Y axis). On the contrary, the x axis corresponds to the circumferential direction.

8.2 Finite element model for the panel

8.2.1 Elements and properties

A simple finite element model is created to represent one panel of the axial cylinder (see Figure 8.2). 4851 two-dimensional elements are used to represent the sheet of metal, more specifically, they are **CQUAD4** elements with an average size of 5.571 N.d. These elements are associated to a **PSHELL** property which models Aluminium 2219-T851 thin plates (see Table 4.1 for material properties). The initial thickness chosen for shell elements is 1 N.d.

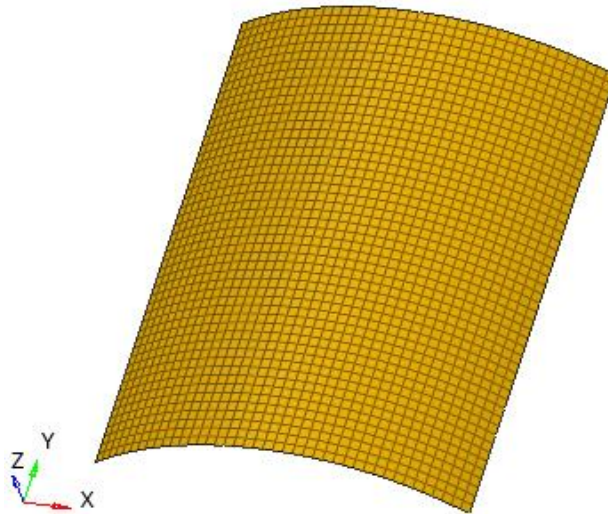


Figure 8.2. Panel finite element model

Due to simplicity of the model, the quality check for mesh has a positive result. All parameters checked for CQUAD4 elements (aspect ratio, warpage, jacobian ratio, minimum and maximum angles, chordal deviation) meet quality criteria recommended by [5].

8.2.2 Constraints

A schematic representation of constraints can be seen in Figure 8.3. Each panel is fastened to the longitudinal longerons on its lateral edges (red coloured), and it is welded to the top and bottom rings on its top and bottom edges, respectively (blue coloured).

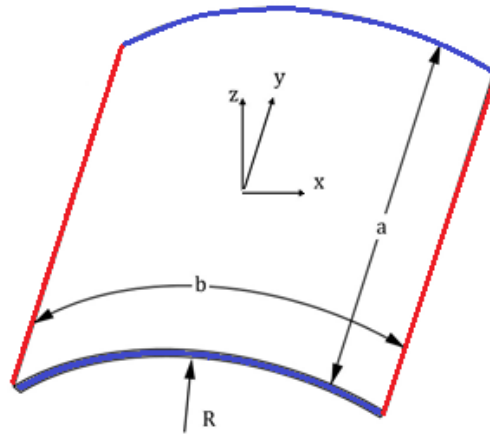


Figure 8.3. Panel connections

As constraints, the welded connections are represented by a pin support, meanwhile bolted edges are represented by a fixed support except for the x axis in order to study buckling. Table 8.1 includes information about fixed degrees of freedom (DOF) for each edge.

Edge	Fixed DOF
Top	13
Bottom	123
Lateral	1346

Table 8.1. Constraints for panel FE model

where,

- DOFs 1, 2, and 3 are x, y, and z translation degrees of freedom.
- DOFs 4, 5, and 6 are x, y, and z rotational degrees of freedom.

8.3 Free size optimization

Free-size optimization has the capability of obtaining the optimized shell thickness. Nevertheless, the purpose of this chapter is to check OptiStruct capabilities to output a stiffened curved panel. Therefore, even if free-size was applied to the panel model described in section 8.1, those results will only be useful as a comparator with the optimized stiffened panels produced by the other optimization procedures.

In all cases, the objective is to minimize the mass within limits of failure modes. The minimum bound for shell thickness is 0.286 N.d. and the maximum is 1.714 N.d. Additionally, a pattern group parameter is defined so that thickness is uniform for the whole plate.

Results for free-size panel optimization will be given when comparison with other optimization types is needed.

8.4 Topology optimization

Topology optimization objective is to find the optimum distribution of material and voids, a so called 0-1 problem, where material either exists or not. For the case of study, a panel with holes is incompatible with pressure containment needed in the space module. But a different definition of the topology problem allows to obtain a rib pattern in the panel.

8. Optimization of a reinforced curved panel

Instead of defining the complete thickness of the shell element as designable, a core non-designable thickness, T_0 , must be provided in addition to a maximum thickness, T , which includes the core thickness and a designable region (where the ribs can be grown). [4]

In Figure 8.4, shell thickness definition is shown.

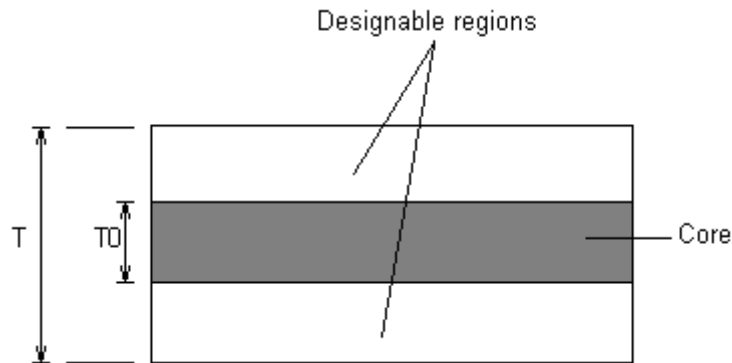


Figure 8.4. Rib pattern definition for topology optimization [4]

The rib patterns can be interpreted by visualization of the density contour plots, as it is still a topology optimization. Wherever the density values reach 1.0, a rib with the height of the core plus the designable thickness is needed. Where the density values go to 0.0, no rib is required and it just retains the core thickness.

Since shell elements are being used, the aspect ratio has to be taken into account. Thickness cannot be greater than the in-plane dimensions of the elements. For this reason, a maximum value of 5.571 N.d. thickness can be reached, as it is the element average size.

It is remarkable that it is not possible to obtain ribs only on one face of the shell elements as T_0 is the mid-layer thickness. Ribs will be symmetric with respect to the mid-layer and will be placed within $[(T_0/2) + (T/2)]$ and $[(-T_0/2) - (T/2)]$ about the shell model.

As a thickness sizing optimization is being developed, it is expected that similar results could be obtained with free-size optimization if not a uniform grouping pattern manufacturing constraint is set. In that case, T and T_0 would be the maximum and minimum thickness values, respectively.

8.4.1 Optimization set up

Optimization model

The optimization model is the curved panel described in section 8.1.

Subcases

The list of subcases studied is the one described in section 5.4 with constraints specified in section 8.2.2.

Objective

The objective of the optimization is to minimize the total mass of the panel. Thus, a mass response must be defined in OptiStruct.

Design variables

Design variables for a topology optimization on shell elements correspond to their thickness. For maximum thickness 0.571 N.d. will be chosen. 0.143 N.d. will be set as the core non-designable thickness for manufacturing reasons.

8. Optimization of a reinforced curved panel

Constraints

In order to check yield strength and global buckling failure modes, two responses will be defined: one for von Mises static stress and another one for buckling.

To introduce maximum and minimum stress constraints, it is necessary to calculate values for which stress response will have at least $MOS = 0$. Taking into account FOSY and design factors already defined, limit values for von Mises constraint are: upper boundaries equal to 176.22 MPa for subcases 1-8 and to 133.50 MPa for subcase 9.

On the other hand, buckling constraint will have a lower boundary of 65 to have buckling as controlling failure mode.

8.4.2 Results

Table 8.2 shows a comparison between topology and unstiffened panel optimization results. MOS are practically the same for both yielding and buckling. However, a reduction of 2.57% of panel mass can be done to the panel when stiffeners are used.

Optimization type		Topology	Unstiffened panel (Free-size)
Mass [kg]		7.57	7.77
Yield Strength	Limiting subcase	9	9
	$\sigma_{VM,max}$ [MPa]	75	76
	MOS_{yield}	0.78	0.76
Global Panel Buckling	Limiting subcase	7	7
	λ_α	64.66	65
	MOS_{buck}	0.005	0

Table 8.2. Stiffened (topology) vs unstiffened (free-size) panel optimization results

The object of this exercise is to determine where to locate ribs in the designable region. The optimized panel is shown in Figure 8.5. Regions that need reinforcement tend towards a density of 1.0. Areas that do not need reinforcement tend towards a density of 0.0. A clear vertical pattern for ribs can be distinguished, with maximum and minimum heights equal to extreme values established for the design variables.

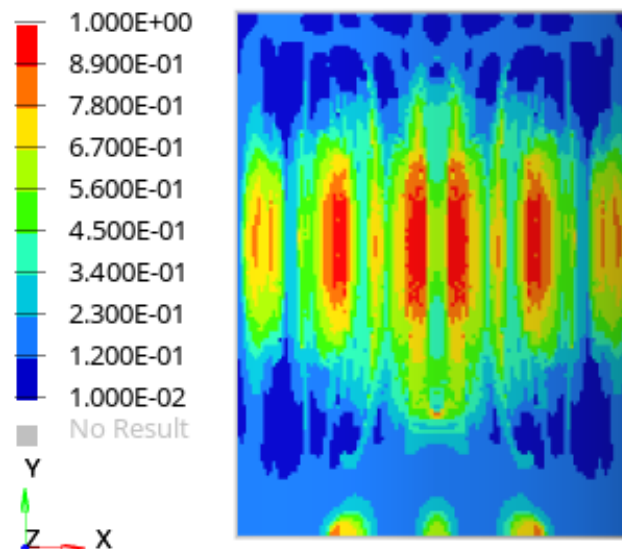


Figure 8.5. Topology optimized panel. Element density values from 0 to 1

8. Optimization of a reinforced curved panel

Figure 8.6 represents buckling shape for first mode of subcase 7 after topology optimization. It is observed how deformations caused by buckling coincide with ribs formation in order to minimize this effect.

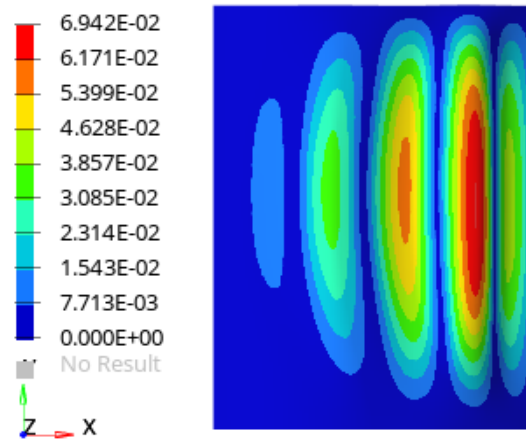


Figure 8.6. Buckling shapes for subcase 7 after topology optimization with displacement contour (m)

Figure 8.7 shows maximum von Mises stresses for the internal pressure case, which is the most critical yielding subcase, before and after topology optimization. Due to the fact that buckling is the controlling failure, it is expected that von Mises results are worse after optimization as they are not limiting the design variables progress. In Figure 8.7 (b), it is remarkable that lowest stress values are found where element densities tend to 0, i.e., there is no need of stiffening. In the central area, where stiffening pattern is drawn, stresses are kept constant.

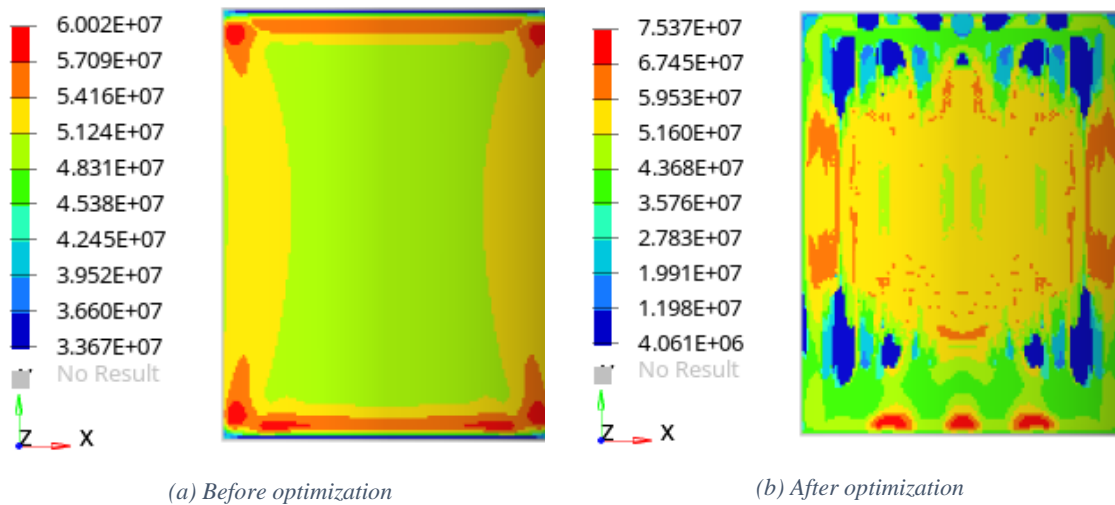


Figure 8.7. Envelope of maximum von Mises stress [Pa] for topology optimization (subcase 9)

Normal modes analysis is included but not constrained in optimization. The first mode is associated to 68.7 Hz, so resonant frequencies will be compliant with what is established in section 5.3 for all axis.

8.5 Topography optimization

Topography optimization is a type of shape optimization in which a pattern of reinforcements within the design region is generated. The purpose of this chapter is to check if OptiStruct can generate a stiffened curved panel whose performance in terms of yielding, buckling or mass is improved.

For this reason, results of topography optimizations will be compared with the optimized unstiffened panel generated using free-size, constrained in the same way as for topology optimization.

Topography optimization is limited because volume and mass responses are not recommended to be introduced as objective or constraints [4]. However, it is possible to combine topography with another optimization types, like free-size, to make it sensible to these responses.

8.5.1 Optimization set up

Optimization model

The optimization model is the curved panel described in section 8.1.

Subcases

The list of subcases studied is the one described in section 5.4 with constraints specified in section 8.2.2.

Design variables

Design variables for a topography optimization correspond to beads formation parameters:

- Bead minimum width. This parameter controls the width of the beads in the model. The recommended value by [4] is between 1.5 and 2.5 times the average element width, therefore it is set to 11.429 N.d.
- Draw angle. It controls the angle of the sides of the beads. The recommended value by [4] is between 60 and 80 degrees. Hence, 60 degrees is chosen not to increase excessively stress concentration, even if the object of this exercise is to determine where and which shape reinforcements should have to improve buckling performance.
- Buffer zone. It allows smooth transition between design and non-design nodes. Buffer zone parameter is activated.
- Draw maximum height. It controls the height of the beads in the model. Draw maximum height is set to 2.857 N.d.
- Normal element method is activated. In this way, beads are intended to be drawn normal to the surface

Cases of study

In order to check capabilities of this optimization type, three cases with different objectives and constraints were studied.

8. Optimization of a reinforced curved panel

	(A)	(B)	(C)
Optimization type	Topography	Topography + free-size	Topography + free-size
Objective	Maximize minimum buckling factor	Maximize minimum buckling factor	Minimize mass
Constraints	Yielding constraint as defined in section 5.6.1	Mass lower than the one for the unstiffened optimized panel	Yielding constraint as defined in section 5.6.1.
			Buckling factor > 65

Table 8.3. Cases of study for topography optimization

On the other hand, buckling constraint will have a lower boundary of 65 to have buckling as controlling failure mode in a similar way as it was for the complete space module optimization.

8.5.2 Results

Results from all cases are shown in Table 8.4.

Optimization case		Topography			Unstiffened panel (Free-size)
		(A)	(B)	(C)	
Mass [kg]		27.64	7.76	8.63	7.76
Yield Strength	Limiting subcase	9	9	9	9
	$\sigma_{VM,max}$ [MPa]	131.91	573	121.30	76
	MOS_{yield}	0.01	-0.77	0.10	1.76
Global Panel Buckling	Limiting subcase	7	7	7	7
	λ_α	1569	248	73	65
	MOS_{buck}	23.14	2.82	0.12	0

Table 8.4. Results for topography optimizations

Case (A) has the best buckling performance, however, that is not needed for the loads present as it can be observed for the large MOS value. In addition, mass is increased more than 350% with respect to the unstiffened panel, which already fulfils all mechanical requirements. Thus, the unstiffened panel would be a clear better option rather than the panel solution obtained from case (A).

For case (B), mass is constrained to the unstiffened panel value. Due to stiffeners produced, buckling MOS is improved, but yield constraint is not fulfilled ($MOS_{yield} < 0$). Nevertheless, stress values should be taken only as a guide, because stiffeners produced with topography optimization are changing shape of the metal sheet. They do not change its thickness to form ribs. Hence, if stiffening must be done by the use of ribs, stresses will be completely different from the topography reinforcements results. They will only help with pattern definition.

Case (C) have better buckling and yielding performances than the unstiffened panel, but an 11% of extra mass is needed.

Figure 8.8 shows shape changes for the three different cases studied. It must be pointed out that all reinforcements are automatically extruded to the inner face of the panel, in the same way as typical waffle stiffeners are located for this kind of structure.

8. Optimization of a reinforced curved panel

For cases (A) and (B), whose objective is maximizing buckling factor, shapes are similar. They show a random pattern that may support the idea of random stiffeners pattern improving buckling performance.

On the contrary, case (C) has a completely different shape change because objective is minimizing mass. Therefore, topography optimization can generate different stiffeners patterns by settling it up depending on designer's principal interest.

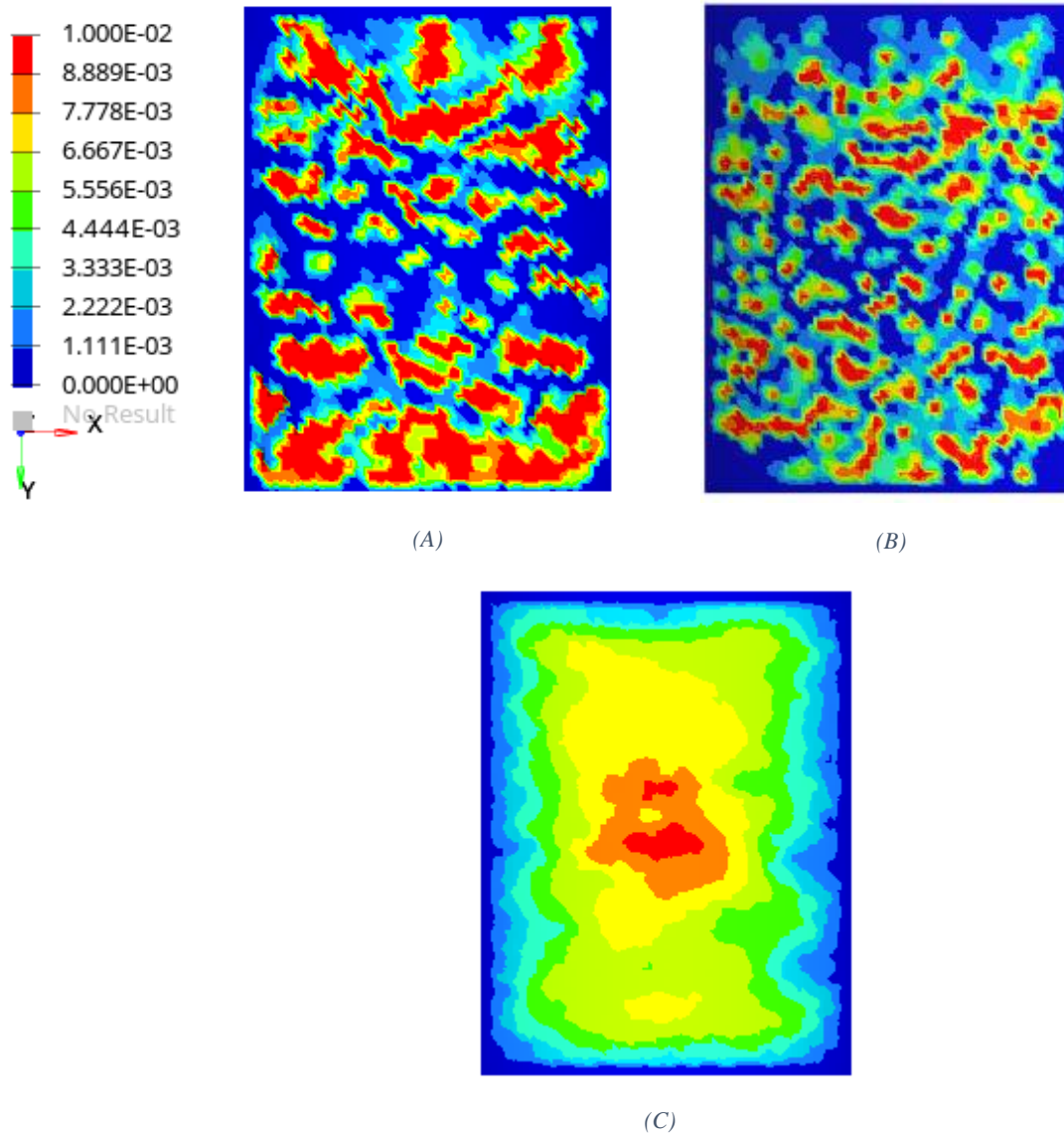


Figure 8.8. Topography optimization shape changes [m]

Figure 8.9 represents buckling shape for first mode of subcase 7, case (B), before and after topography optimization. It is observed how shape optimization blurs deformations caused by buckling.

8. Optimization of a reinforced curved panel

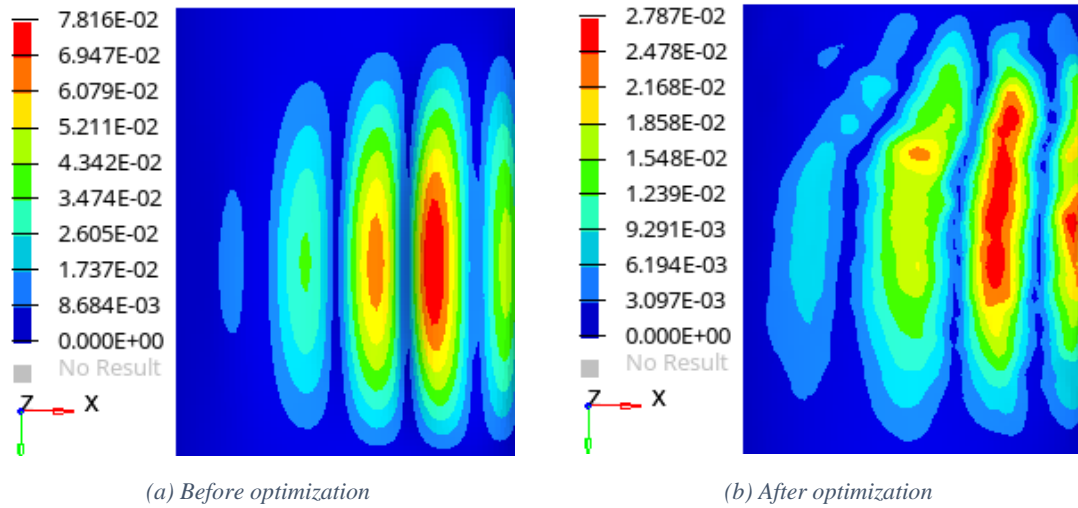


Figure 8.9. Buckling shapes for subcase 7, case (B), along topography optimization with displacement contour (m)

Even if stresses results are not that relevant for the objective of the present work, it is remarkable how different they are for the three cases. See Figure 8.10. For cases (A) and (B), stresses are distributed along the surface without any pattern, similar to reinforcements location. However, case (C) has the lowest von Mises stresses and they are located in the vertical edges of the panel.

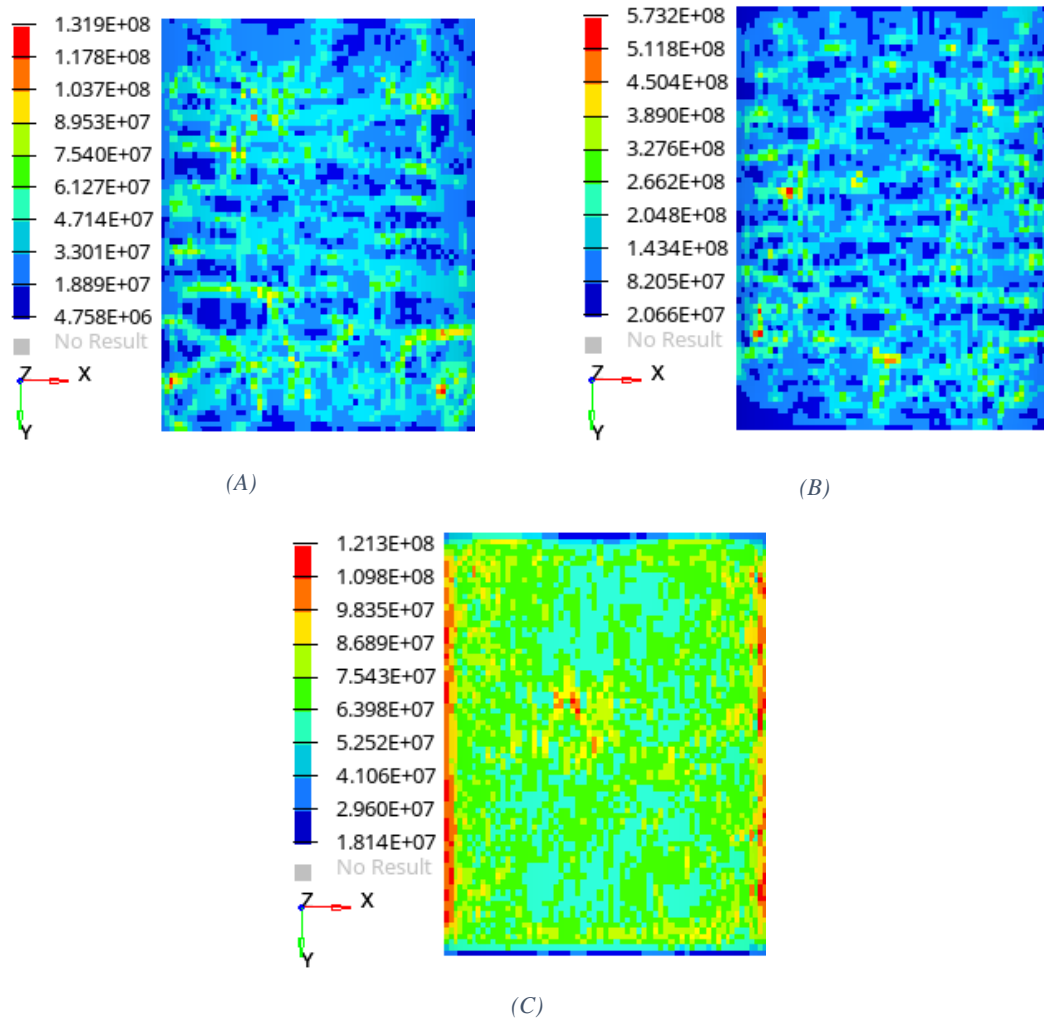


Figure 8.10. Topography optimization stress results [Pa]

8. Optimization of a reinforced curved panel

Normal modes analysis is included but not constrained in optimization. The first mode is associated to 73.2 Hz, so resonant frequencies will be compliant with what is established in section 5.3 for all axis.

In addition, it must be reminded that manufacturing constraints can be added to topography optimization. For example, beads can be constrained to be linear following a user-defined direction as it is shown in Figure 8.11.

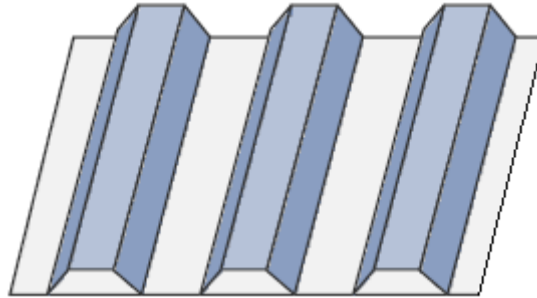


Figure 8.11. Linear manufacturing constraint example [4]

8.6 Free-shape optimization

A free-shape optimization consists on modifying the outer boundary of the structure to find the optimal shape. Its allowable movement is automatically determined, so it is sufficient to choose a set of nodes on the boundary.

In section 3.3, it was said that shape change is performed in a different way depending on the element type of the FE model. As extruded stiffeners from the panel are needed, it is not possible to run the optimization with the FE model formed by shell elements (2D elements). Thus, solid elements (3D elements) will be used so that grids move normal to the surface.

Experience and literature suggest that for a thin-walled cylinder, radius to thickness ratio (R/t) larger than 25 [17], it becomes increasingly uneconomical to use solid elements because several layers of elements are required to model the through-thickness stress distribution properly. The structure under study has a R/t larger than 600, therefore shell elements are strongly recommended.

However, free-shape optimization will be developed with different layers of solid elements, in order to check whether this type of optimization is valid for obtaining a stiffened curved panel.

8.6.1 Optimization set up

Optimization model

The optimization model is the curved panel described in section 8.1. Nevertheless, in this case, a FE model with **SOLID** elements with an average size of 0.286 N.d. will be used. These elements are associated to a **PSOLID** property which models Aluminium 2219-T851 thin plates (see Table 4.1).

Subcases

The list of subcases studied is the one described in section 5.4 with constrains specified in section 8.2.2.

8. Optimization of a reinforced curved panel

Objective

The objective of the optimization is to minimize the total mass of the panel. Thus, a mass response must be defined in OptiStruct.

Design variables

Shape variables are not needed as free-shape optimization automatically does it. However, it is possible to constrain extrusion of reinforcements to go to the inner face of the panel, in the same way as typical waffle stiffeners are located for this kind of structure.

Constraints

In order to check yield strength and global buckling failure modes, two responses will be defined: one for von Mises static stress and another one for buckling.

To introduce maximum and minimum stress constraints, it is necessary to calculate values for which stress response will have at least $MOS = 0$. Taking into account FOSY and design factors already defined, limit values for von Mises constraint are: upper boundaries equal to 176.22 MPa for subcases 1-8 and to 133.50 MPa for subcase 9. If stresses go higher than these values, yielding will occur.

On the other hand, buckling constraint will have a lower boundary of 65 to have buckling as controlling failure mode.

Cases of study

Three different models will be used with one, two and four layers of solid elements forming the panel thickness.

8.6.2 Results

Table 8.5 includes results of the cases of study and the optimized unstiffened panel obtained from free-size optimization in order to compare data.

Optimization case		Free-shape			Unstiffened panel (Free-size)
		1 layer	2 layers	4 layers	
Mass [kg]		9.76	7.18	7.17	7.76
Computing time [min]		237	200	908	28
Yield Strength	Limiting subcase	9	9	9	9
	$\sigma_{VM,max}$ [MPa]	133.5	116	127	76
	MOS_{yield}	0	0.15	0.05	1.76
Global Panel	Limiting subcase	7	7	7	7
	λ_α	89	64.99	65	65
Buckling	MOS_{buck}	0.37	≈ 0	0	0

Table 8.5. Results for free-shape optimizations

Although optimizations have the same parameters, results are different for the three cases due to the accuracy that extra element layers provide.

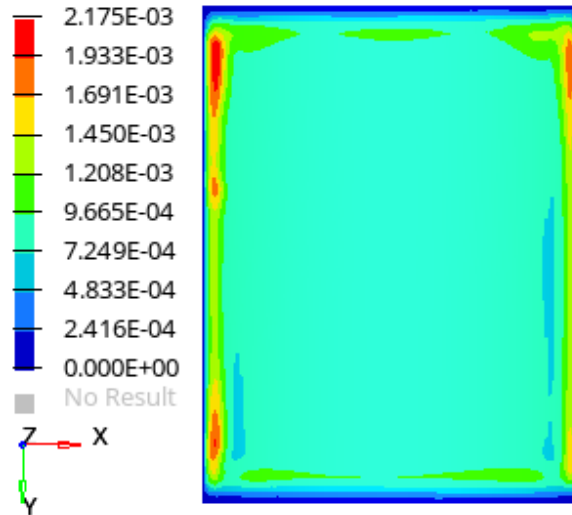
With only one layer of elements, yielding becomes the controlling failure mode (MOS_{yield} equal to 0), which is incoherent with constraints applied and results for the free-size optimization. It is clear that stress distribution is not properly calculated as it was predicted in [17]. Thus, this 1-element-layer model is not reliable.

8. Optimization of a reinforced curved panel

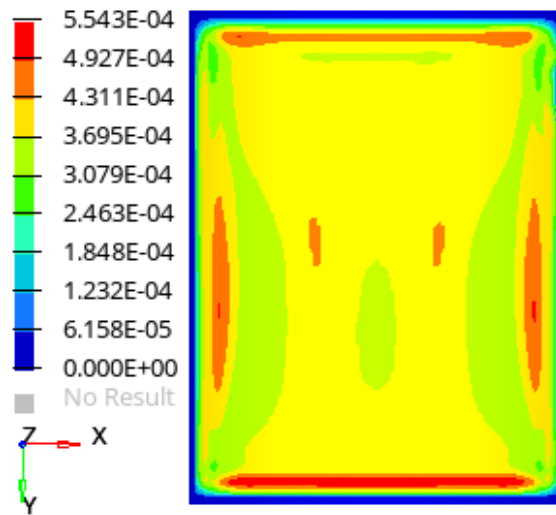
For the cases of 2 and 4 element layers, buckling mode is the critical one (MOS_{buck} equal to 0), as expected. Besides, in both cases, mass is reduced with respect to the unstiffened optimized panel produced by free-size. Consequently, von Mises stresses increase, but within the limits (positive MOS_{yield}). Therefore, shape changes proposed could be a feasible solution to reduce mass when mechanical requirements are fulfilled by adding reinforcements.

When increasing number of element layers, results seem to start converging. The same occurs with shape changes proposed for these cases, which can be seen in Figure 8.12 (b)-(c). Small reinforcements (0.5 - 0.6 mm height) are shaped in the vertical and horizontal edges of the panel. However, the 4-element-layer pattern suggests that more delimited stiffeners could be shaped when increasing layers. The disadvantage of adding more solid layers is the computing time. When doubling layers from two to four, computing time was increased a 354%. So, it depends on designer if these time-consuming models are worth to be developed or not.

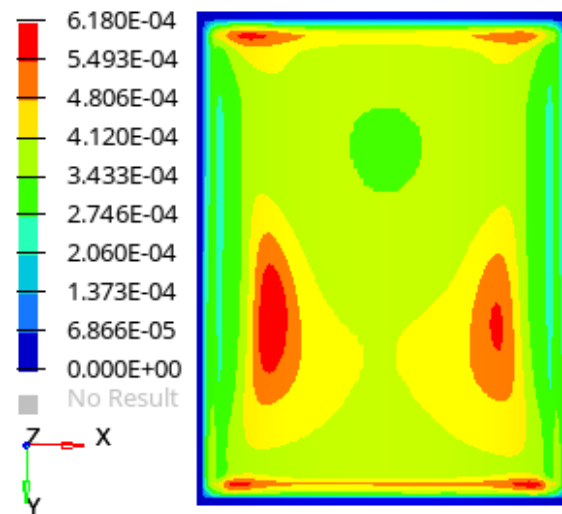
8. Optimization of a reinforced curved panel



(a) 1 layer of elements



(b) 2 layers of elements

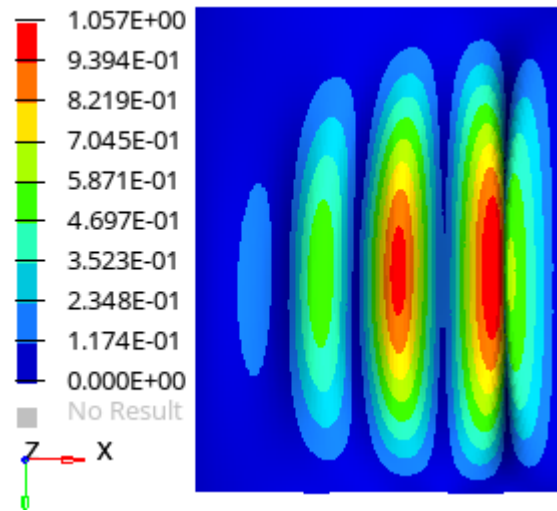


(c) 4 layers of elements

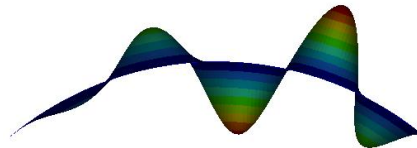
Figure 8.12. Free-shape optimization shape changes [m]

8. Optimization of a reinforced curved panel

Buckling shapes generated by the 4-layer model are worth commenting. See Figure 8.13. As MOS_{buck} is exactly 0, buckling starts, so huge deformations are produced due to failure.



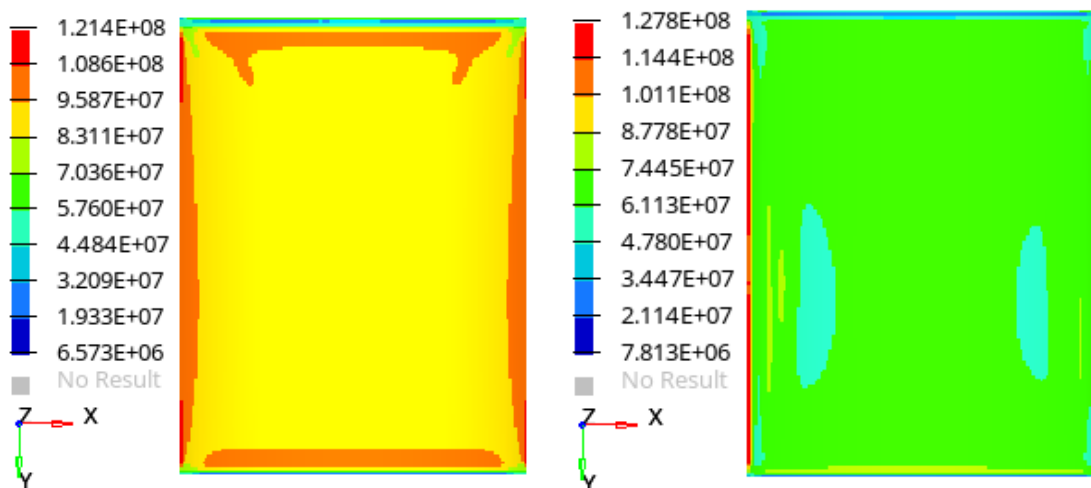
(a) Front view



(b) Top view

Figure 8.13. Buckling shapes for 4-layer model after free-shape optimization (subcase 7)

Regarding stress distribution, Figure 8.14 shows results for the 4-layer model before and after the free-shape optimization. Although magnitudes are not changing too much, it can be observed that stress concentration for the optimized model is in the vertical edges where panels are jointed to the longerons, meanwhile the central area average stress is considerably reduced.



(a) Before optimization

(b) After optimization

Figure 8.14. Free-shape optimization stress results for 4-layer model [Pa] (subcase 9)

8. Optimization of a reinforced curved panel

Normal modes analysis is included but not constrained in optimization. The first mode is associated to 71.1 Hz, so resonant frequencies will be compliant with what is established in section 5.3 for all axis.

In the same way as for topography, pattern manufacturing constraints can be added for free-shape optimizations to produce specific shaped reinforcements. Another alternative could be to directly create the shape variables using shape optimization.

9 Conclusions

In the present thesis work, optimization of the axial cylinder of a pressurized manned module has been developed by using OptiStruct. Two optimization approaches are employed for the unstiffened and reinforced panel. In both cases definition of optimization parameters is done. Design loads have included launch accelerations and maximum expected operative pressure. Optimization constrains have been expressed as positive MOS for global instability and strength failure modes. Several optimization cycles have concluded in the optimum model.

The unstiffened panel is optimized by using free-size method in which only shell thickness is modified. The FE model used corresponds to the complete pressurized space module, which considerably has increased computing time. However, by using the full FE model, results are reliable, overcoming differences by using the FEM.

Problem set up is simple, e.g., definition of analysis, optimization areas and other optimization parameters. Computing time is not excessive, but adequate. Finally, optimized unstiffened plate is obtained with a reduction of mass and fulfilling all mechanical requirements.

When comparing HyperSizer and OptiStruct results for the same model used in [1] and the present work, respectively, differences arise. Not the same optimum thickness is obtained. Apart from differences on failure modes definitions, the fact that FEA are not updated for each iteration is an approximation done in [1] that could lead to inaccurate results. Moreover, HyperWorks allows user to work with only one interface, instead of using Nastran and HyperSizer.

On the contrary, HyperSizer capability for condensing FEA results turns extremely useful when models are so large that computing time without simplification becomes increasingly uneconomical. Furthermore, HyperSizer ability for updating KDF in each iteration for buckling analysis is lacking in OptiStruct.

With respect to the stiffeners designs for the simple curved panel model, all, topology, topography and free-shape optimization methods, come up with different possible patterns. However, several iterations are needed in order to define the proper optimization set up. In the present work, just final optimizations are included.

Topology method obtained vertical reinforcements that were able to reduce panel mass with respect to the unstiffened optimized panel without compromising structural integrity. But well-defined ribs are not possible to be obtained as it is basically a thickness shell optimization and in order to produce a fine rib with this parameter, each element thickness should be constrained separately. Nevertheless, some manufacturing constraints could be implemented, like symmetry, to obtain an easier-to-manufacture pattern.

If user decides that stiffeners design is acceptable, then OSSmooth tool from HyperMesh can be used to generate a FE model based on the resulting design and proceed with designing progress.

Topography optimization involves many bead parameters to be defined, which makes optimization definition process longer. However, interesting resulting were obtained as an apparently random pattern of reinforcements is suggested. For the studied cases, distinct objective formulation produces totally different shapes, so depending on designer's priority, topography can be used for optimizing a panel. Besides, manufacturing constraints can be applied to obtain well-defined stiffeners, e.g., linear or symmetrical pattern.

9. Conclusions

A disadvantage is that reinforcements are simply changes of shape, they are not adding material, so OSSmooth cannot be used to generate the optimized model in HyperMesh for a reanalysis.

Free-shape approach is able to produce a stiffeners pattern which is able to reduce panel mass with respect to the unstiffened optimized panel without compromising mechanical integrity. Despite this, this method requires high computing time because of the use of solid elements, which are still not proven to be reliable in terms of stress performance.

However, if free-shape method is considered, manufacturing constraints can be added to obtain a well-defined reinforcement shape, e.g., member size control, side constraints or some symmetrical pattern. Then OSSmooth tool from HyperMesh can be used to generate a FE model based on the output design and proceed.

In general, OptiStruct, and so HyperWorks suite, is a powerful optimization tool that allows designer to work along the whole mission process. Firstly, it is possible to obtain optimized results when there are no limitations for the output, like the research made for stiffening methods for curved panels. This capability extremely increases designer possibilities. Secondly, a preliminary design can be done by using free-size, free-shape or topology optimization, which still have wide margin for modifications. Lastly, it is possible to add many constraints so that manufacturing feasibilities are granted for the optimized detailed design.

Even though Altair Engineering provides users with guides, tutorials, forums and courses, OptiStruct capabilities can be adapted to any optimization problem, from the simplest to the most complicated and specific ones. Therefore, it is impossible to know in advance all possibilities for a concrete structure design problem.

Moreover, working with a complete suite facilitates communication between programmes, making sure that no information will be lost, and it makes easier for the user to work with the different tools as interfaces and capabilities are similar and connected.

In conclusion, OptiStruct is a powerful optimization tool with limitless options for any kind of structural problem. It can help design engineer at different mission states and provide him with new shape designs that has never thought about.

Appendix A. Finite element model of module

In this chapter the FE model of the module is described. The FE model was provided by Thales Alenia Space as a result of a master thesis developed at Politecnico di Milano by Virtudes de Gregorio Roig [1]. Checks for the FE model can be found in the mentioned work. For the scope of this work, the FE model will be considered already checked.

A summary of elements and properties used is given in Table A.1. The terminology employed is typically used in FEM. It is widely described in HyperMesh User's Guide [5].

Type of element	Number	Characteristics
CBEAM	742	1D element. It supports tension, compression, axial torsion and bending.
CBUSH	104	1D element. It can generate a link between not coincident nodes and recover the resultant element forces for bolts verification.
CONM2	3	0D element. It is a concentrated mass.
CQUAD4	75,694	2D element. It can model in-plane, bending, and transverse shear behaviour.
CTRIA3	635	2D element. It can model in-plane, bending, and transverse shear behaviour.
RBE2	789	1D element. It represents an idealized rigid connection to transmit loads between interfaces.
RBE3	3	1D element. It is an interpolation element, but it is not rigid. It does not add any stiffness between the independent and dependent nodes, but loads are transferred.
Total	77,970	-
Type of property	Number	-
PBEAML	1	-
PBUSH	1	-
PSHELL	26	-

Table A.1. FE model summary

Most of the structure geometry is represented using two-dimensional elements, CQUAD4 and CTRIA3. From all the two-dimensional elements, 99% are CQUAD4, with average size equal to 20 mm. Meanwhile, CTRIA3 triangular elements are mainly used for mesh transitions or for modelling portions of the structure when quadrilateral elements are impractical. Both, CQUAD4 and CTRIA3 elements, are associated to a PSHELL property modelling Aluminium 2219-T851 thin plates of different thicknesses.

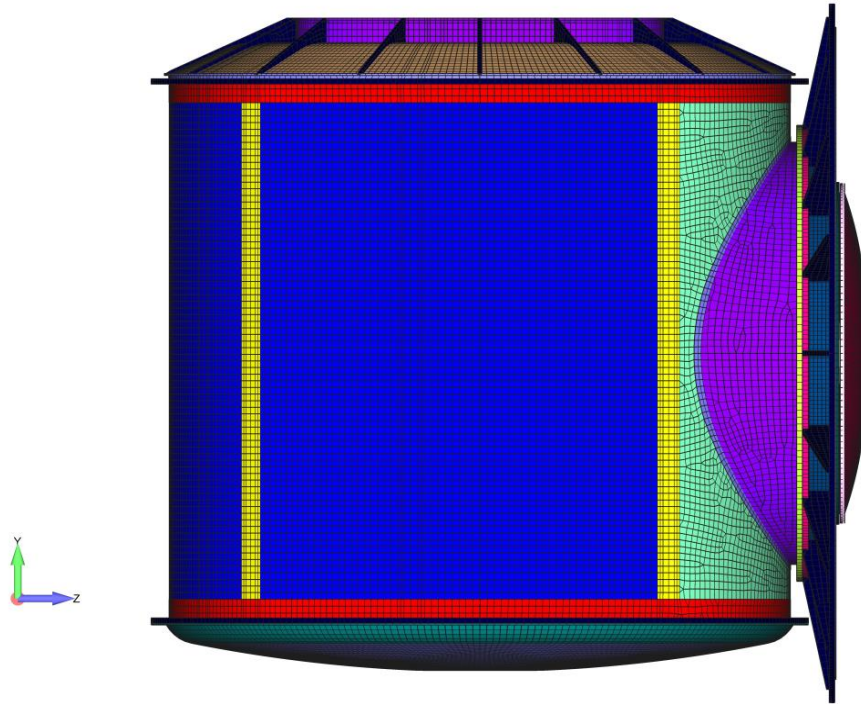


Figure A.1. Lateral view of the FE model [1]

In general, CQUAD4 elements are more accurate than CTRIA3 elements, because the latter may exhibit excessive stiffness, particularly for membrane strain. Nevertheless, quadrilateral elements should be kept as nearly square as possible, and triangular elements should be kept as nearly equilateral as possible. This is due to deterioration of accuracy when their aspect ratio increases as described in [5].

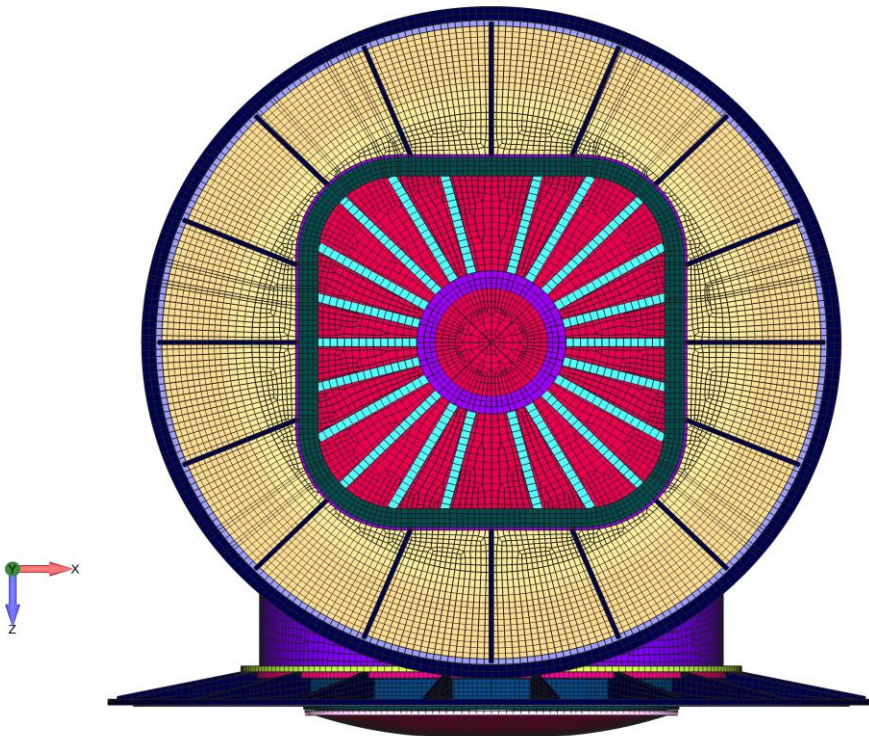


Figure A.2. Top view of the FE model [1]

Regarding the element size, it has been selected according to Thales Alenia Space recommendations for the type of analysis and dimensions. It is a compromise between accuracy of the finite element analysis results and the solution computing time.

The hatches ribs are simplified and represented by CBEAM elements (coloured in light blue in Figure A.2). They are associated to a PBEAML property used to define the L-cross-section shape.

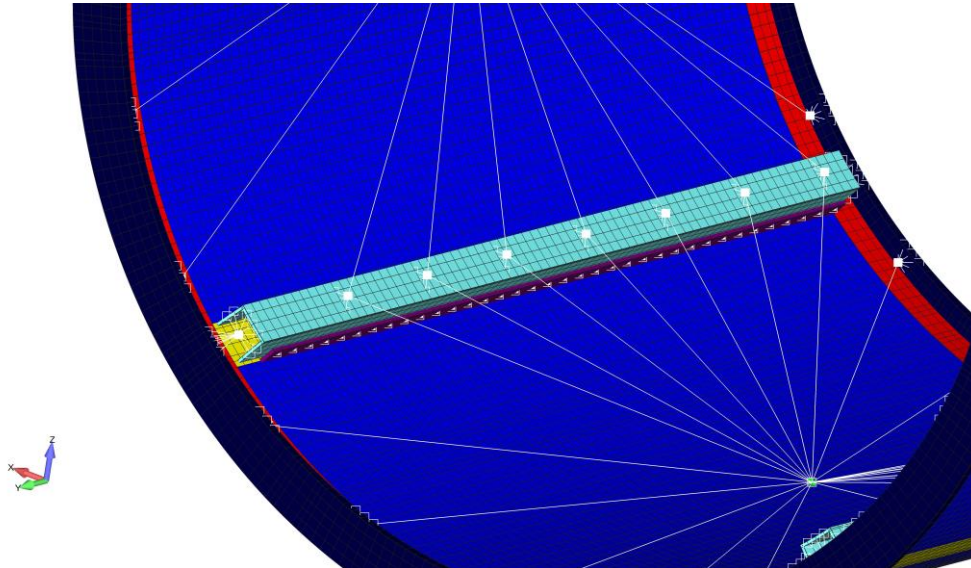


Figure A.3. Detailed view of longerons attachments and secondary masses connections [1]

Figure A.3 shows a detailed view of the rigid elements (coloured in white) used to represent connections between parts. The longerons and the axial cylinder ribs are fastened by using RBE2 rigid elements. In correspondence of the fasteners, the nodes at the ribs are defined as independent and all 6 DOF of the nodes at the longerons are made dependent. The same type of elements is used to model the interface structure that connects longerons to the top and bottom rings. In this case, an independent grid point is used to represent the interface and all 6 DOF of a set of nodes at the end of longerons and at rings in correspondence of the connection are defined as dependent. RBE2 elements simplify the representation of the mentioned interfaces, which are complex to model in detail. Therefore, results in the proximity of these links should not be trusted as an artificial rigidity may be introduced in the model. For the final design, it is required to develop a detailed model and a fine mesh to capture local effects, which is out of the scope of the present work.

In addition, RBE2 elements are used to model the interface between the axial bulkhead and the axial hatch and between the access closure and the radial hatch. These interfaces must secure the pressure containment, hence the rigidity introduced by RBE2 elements is adequate.

Three CONM2 elements are used to model the secondary masses, which are described in section 4.1. The total mass budget is divided equally between those three elements, which are associated to one panel each and are located at nodes in correspondence of the centre of gravity of the axial cylinder segments (see Figure A.3). Brackets are used to connect them to the longerons of the primary structure and they are represented by RB3 elements that transfer the secondary masses inertial loads to the primary structure. The RB3 elements define the motion of the CONM2 nodes (dependent) as the weighted average of the motions at the set of grid points representing brackets (independent). Then, RBE2 are used to model the joints of brackets with longerons and rings. For

Appendix A. Finite element model of module

this, the nodes representing brackets are defined as independent whereas the 6 DOF of a set of nodes in correspondence of the attachment to longerons and rings are defined dependent. [1]

The bottom ring and the access closure and the radial ring and the airlock interface are fastened. Those bolts are modelled using CBUSH elements and can be seen in Figure A.4. They are defined using a PBUSH property with six stiffness values, three translational and three rotational. The bolt stiffness determines the way load is transferred from one component to another. Even if there are different formulations extracted from literature, like those by Huth (1986) or Tate (1946), for computing stiffness values, as a preliminary design, it is enough to use rigidity values sufficiently high to emulate a rigid connection, but not so high to cause ill-conditioning of the stiffness matrix. The values of rigidity chosen are the ones recommended by Thales Alenia Space: $k_T = 10^{10}$ N/m for translational stiffness and $k_\theta = 10^8$ N·m for rotational stiffness. The absence of ill-conditioning has been checked as part of the FEM checks activities done in the reference master thesis developed by Virtudes de Gregorio Roig [1] where the model was extracted from.

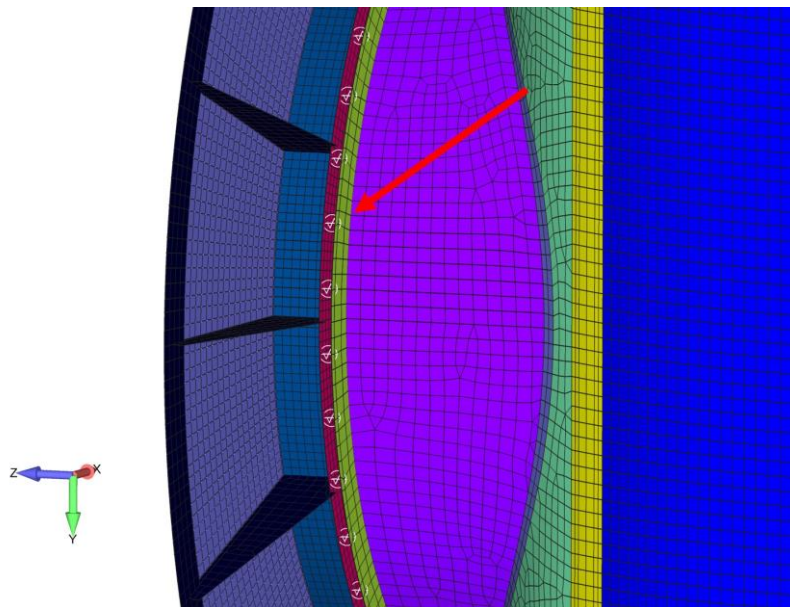


Figure A.4. Detailed view of CBUSH elements (in white) [1]

References

- [1] V. De Gregorio Roig, “Structural Analysis and Optimization of a Pressurized Manned Module,” Politecnico di Milano, 2020.
- [2] P. W. Christensen and A. Klarbring, *An introduction to structural optimization - Solid Mechanics and its Applications*, vol. 153. Linköping, Sweden: Springer Science + Business Media B.V., 2009.
- [3] A. Olason and D. Tidman, “Methodology for Topology and Shape Optimization in the Design Process,” Chalmers University of Technology, 2010.
- [4] Altair, “Altair OptiStruct 2021 User Guide,” 2021.
- [5] Altair, “Altair HyperMesh 2021 User Guide,” 2021.
- [6] M. Zhou, Y. K. Shyy, and H. L. Thomas, “Checkerboard and minimum member size control in topology optimization,” *Struct. Multidiscip. Optim.*, vol. 21, no. 2, pp. 152–158, 2001, doi: 10.1007/s001580050179.
- [7] O. Sigmund and J. Petersson, “Numerical instabilities in topology optimization: A survey on procedures dealing with checkerboards, mesh-dependencies and local minima,” *Struct. Optim.*, vol. 16, no. 1, pp. 68–75, 1998, doi: 10.1007/BF01214002.
- [8] R. C. Rice, J. L. Jackson, J. Bakuckas, and S. Thompson, “Metallic Materials Properties Development and Standardization (MMPDS),” U.S. Department of Transportation, Federal Aviation Administration, 2003.
- [9] Arianespace, *Ariane 5 - User’s manual*, no. 5, Rev. 3. Arianegroup, 2020.
- [10] European Cooperation for Space Standardization, *Space engineering: Structural general requirements, ECSS-E-ST-32C Rev. 1*. Noordwijk, The Netherlands: ESA Requirements and Standards Division, 2008.
- [11] G. C. Nelson, *Pressurized Payloads Interface Requirements Document: International Space Station Program*, Revision R. Houston, TX: NASA Johnson Space Center, 2015.
- [12] European Cooperation for Space Standardization, *Structural factors of safety for spaceflight hardware, ECSS-E-ST-32-10C*. Noordwijk, The Netherlands: ESA Requirements and Standards Division, 2019.
- [13] European Cooperation for Space Standardization, *Space engineering: Structural design and verification of pressurized hardware, ECSS-E-ST-32-02C Rev. 1*. Noordwijk, The Netherlands: ESA Requirements and Standards Division, 2008.
- [14] European Cooperation for Space Standardization, *Space engineering: buckling of structures, ECSS-E-HB-32-24A*. Noordwijk, The Netherlands: ESA Requirements and Standards Division, 2010.
- [15] J. E. R. Johnston, J. T. DeWolf, D. F. Mazurek, and F. P. Beer, *Mechanics of materials*, 6th ed. McGraw-Hill, 1981.
- [16] V. I. Weingarten, P. Seide, and J. P. Petersson, “Buckling of Thin Walled Circular Cylinders,” NASA Langley Research Center, NASA SP-8007, 1965.
- [17] A. J. Sadowski and J. M. Rotter, “Solid or shell finite elements to model thick cylindrical tubes and shells under global bending,” *Int. J. Mech. Sci.*, vol. 74, pp. 143–153, 2013.

